

# Probing the Light Quark Sea Flavor Asymmetry With Semi-inclusive Charged Pion Production in Hall C

July 7, 2006

W. Chen, D. Dutta, H. Gao (Spokesperson/Contact person), K. Kramer,  
X. Qian, Q. Ye, X. F. Zhu, X. Zong  
*DUKE UNIVERSITY*

E. Christy, C. Keppel, V. Tvaskis  
*HAMPTON UNIVERSITY*

J. Dunne, D. Dutta  
*MISSISSIPPI STATE UNIVERSITY*

C. Glashausser, R. Gilman, X. D. Jiang, G. Kumbartzki, R. D. Ransome,  
*RUTGERS UNIVERSITY*

H. Avakian, P. Bosted, A. Bruell (Spokesperson), J. P. Chen, R. Ent, M. Jones  
*THOMAS JEFFERSON NATIONAL ACCELERATOR FACILITY*

E. R. Kinney  
*UNIVERSITY OF COLORADO*

J. C. Peng, L. Y. Zhu  
*UNIVERSITY OF ILLINOIS, URBANA-CHAMPAIGN*

E. J. Beise, H. Breuer  
*UNIVERSITY OF MARYLAND*

A. Asaturyan, R. Asaturyan, A. Mkrtchyan, H. Mkrtchyan (Spokesperson), T.  
Navasardyan, V. Tadevosyan  
*YEREVAN PHYSICS INSTITUTE, ARMENIA*

## Abstract

We propose to measure the differential cross section of the semi-inclusive ( $e, e'\pi^\pm$ ) reaction from both the hydrogen and deuterium targets in the kinematic range of  $0.1 < x < 0.48$ ,  $1.2 < Q^2 < 4.3$  (GeV/c) $^2$ ,  $2.3 < W < 3.2$  GeV and  $0.3 < z < 0.7$  in Hall C at JLab with a 11 GeV electron beam. The charged pion yield ratio may be related to  $(d + \bar{d})/(u + \bar{u})$ ,  $(d - \bar{d})/(u - \bar{u})$ ,  $(\bar{d} - \bar{u})/(u - d)$  and favored and unfavored fragmentation function ratio assuming factorization. The factorization assumption seems to be supported by a number of experiments in kinematic regions relevant to the proposed experiment. The precise measurement of these quantities may provide constraints in understanding the nucleon sea quark flavor asymmetry. With a large  $z$  coverage and high precision data, the proposed measurement can also provide a precise test of leading-order factorization assumption. The extracted  $\bar{d}/\bar{u}$  results will have an improved statistical precision at large  $x$  to that of the Fermi Lab E866 Drell-Yan data, providing an independent study of the nucleon sea flavor asymmetry employing a different physical process at very different  $Q^2$  values. Parasitically, the differential cross-section from the semi-inclusive ( $e, e'K^\pm$ ) process will also be measured which allows for an investigation of the leading-order factorization assumption for kaon production and the flavor dependence of the fragmentation functions through charged kaon Semi-inclusive Deep Inelastic Scattering production. In particular, it may provide information on the kaon fragmentation function ratio  $D_d^K/D_u^K$  which hasn't been studied so far in experiments. We request a total number of 52 days for this experiment.

## Collaboration Commitments

The Yerevan group with Hamlet Mkrtchyan as one of the spokespersons of this proposal will take on the responsibility of assembling and testing the calorimeter for the SHMS. The Duke group plans to take on the responsibility of commissioning SHMS detectors relevant for the electron/pion identification.

# Contents

<b>1</b>	<b>Introduction</b>	<b>4</b>
<b>2</b>	<b>Physics Motivation</b>	<b>5</b>
2.1	Flavor asymmetry of the nucleon sea . . . . .	5
2.2	Factorization in parton models . . . . .	7
2.3	SIDIS cross section at leading order and the next-to-leading order . .	8
2.4	Sea quark flavor asymmetry extraction: leading-order method I . . .	10
2.5	Sea quark flavor asymmetry extraction: leading-order method II . .	12
2.6	NLO QCD correction and NLO global fits . . . . .	13
2.7	Charged kaon production in SIDIS . . . . .	13
2.8	Indications of leading order $x - z$ factorization by existing data . .	14
<b>3</b>	<b>Experiment</b>	<b>16</b>
3.1	Experimental overview . . . . .	16
3.2	Choice of kinematics . . . . .	17
3.3	Spectrometer systems . . . . .	21
3.3.1	The electron arm: SHMS . . . . .	21
3.3.2	The hadron arm: HMS . . . . .	23
3.4	Trigger, time-of-flight resolution . . . . .	25
3.5	Target and luminosity normalization . . . . .	25
3.6	Events and background rates estimation . . . . .	28
3.7	Running time allocation and choice of luminosity . . . . .	29
3.8	Systematics uncertainties . . . . .	32
3.9	Projections . . . . .	34
<b>4</b>	<b>Summary</b>	<b>39</b>
<b>5</b>	<b>Acknowledgment</b>	<b>39</b>
<b>6</b>	<b>Appendix A: Single rates on HMS and SHMS</b>	<b>40</b>
<b>7</b>	<b>Appendix B: Projections of Method I</b>	<b>44</b>

# 1 Introduction

Semi-Inclusive Deep Inelastic Scattering (SIDIS), where a hadron is detected in coincidence with the scattered electron, offers insight into the nucleon structure of the nucleon that is unavailable in inclusive DIS which has been the major experimental tool to measure the polarized and unpolarized nucleon structure functions. High momentum fragments of deep-inelastic nucleon breakup may statistically tag the underlying quark flavor structure. For example, SIDIS can access several novel parton distribution functions and fragmentation functions, such as transversity parton distribution functions and the Collins fragmentation functions [1].

An example for these studies is the determination of the light quark sea flavor asymmetry in the nucleon [2]. By measuring  $\pi^+$  and  $\pi^-$  Deep Inelastic Scattering (DIS) yields on hydrogen, deuterium targets, the results on the  $\bar{d} - \bar{u}$  have been reported [3] by the HERMES collaboration through the studies of the flavor decomposition of the unpolarized parton distributions. Their results demonstrated sensitivity in extracting the light sea quark flavor asymmetry with a different process (SIDIS) from the Drell-Yan [4] process in a very different  $Q^2$  region. Hydrogen and deuterium targets are needed in this decomposition, while nuclear corrections to antiquark distributions extracted from the deuteron data are typically less than 1 – 2% for an  $x$  range of 0.1 – 0.4 [5].

A crucial assumption in the extraction of parton distributions is the validity of the QCD factorization of the SIDIS process. The QCD factorization ensures the universality of the parton distribution function among different hard processes. On the theory side, the QCD factorization theorem for SIDIS for fixed values of hadron transverse momentum ( $P_{hT}$ ) has not been proved, while such factorization theorems exist for the integrated functions [6]. To interpret experimental data which do not have full coverage of  $P_{hT}$ , a factorization assumption based on parton model has been adopted instead. The assumption is that the SIDIS process can be factorized into three parts: a parton distribution part, a hard scattering amplitude and a fragmentation part. The tree-level (LO) result up to order  $1/Q$  for leptonic SIDIS has been derived [7]. Even at the tree-level, the cross section still can not be written as a product of parton distribution functions (which depend only on  $x$ ) and fragmentation functions (which only depend on  $z$ ) because of the limited  $P_{hT}$  range. Certain assumptions about the transverse momentum dependence of parton distribution function and fragmentation function have to be made in order to achieve the  $x-z$  factorization. In the NLO (QCD improved parton model), the naive  $x-z$  factorization breaks down because gluon distribution enters the cross section at the  $O(\alpha_s)$  level.

Recently, JLab Hall C E00-108 [8] experiment and the CLAS collaboration [9] reported the evidence supporting the LO  $x - z$  factorization with a 6 GeV electron beam. HERMES [3] reported earlier evidence for the LO  $x - z$  factorization in the kinematic region of  $1.33 < Q^2 < 4.88$  (GeV/c) $^2$  and  $W > 2.0$  GeV. In the proposed experiment, one may further test the factorization assumption by examining the  $z$ -dependence of the extracted parton distribution function. With the large luminosity available at Jefferson Lab with a 11 GeV beam, a detailed separation of the  $x$  and  $z$  dependence of the pion production cross-section will be possible, allowing for an

independent study of the LO  $x - z$  factorization properties <sup>1</sup>.

We propose to carry out a high statistics SIDIS electron scattering experiment at Hall C. There are three major goals of the proposed experiment. First, a new measurement of the nucleon sea-quark flavor distribution difference,  $\bar{d} - \bar{u}$  will be obtained with an improvement of a factor 20 over the HERMES measurement, extending to much higher  $x$  region. Second, the extracted  $\bar{d}/\bar{u}$  results will have an improved statistical precision in the larger  $x$  region compared to that of the Fermi Lab E866 data [4], providing confirmation from an independent physical process on the observed decrease of this ratio with increasing  $x$  at  $x > 0.15$ . Lastly, this experiment will provide the most precise information on the  $d_v/u_v$  ratio. In addition, the proposed experiment will also provide a flavor-dependent kaon fragmentation function ratio and a test of the LO  $x - z$  factorization for both the kaon and pion SIDIS electroproduction.

## 2 Physics Motivation

### 2.1 Flavor asymmetry of the nucleon sea

The earliest parton models assumed that the proton sea was flavor symmetric. In perturbative QCD, the nucleon sea arises from gluon splittings  $g \rightarrow q\bar{q}$ , so symmetry is expected in the distribution of sea quarks and anti-quarks, and also  $\bar{u}(x) = \bar{d}(x)$ . The earliest parton distribution function parameterizations assume these symmetries. However, the non-perturbative dynamics which corresponds to long-range interactions may lead to a sea flavor asymmetry [11].

The first experimental evidence for the inequality of  $\bar{u}(x)$  and  $\bar{d}(x)$  was from a test of the Gottfried Sum Rule, based on a comparison of the inclusive DIS measurements on the proton and the “neutron”. The Gottfried integral [12] is defined as:

$$I_G = \int_0^1 [F_2^p(x, Q^2) - F_2^n(x, Q^2)] \frac{dx}{x} \quad (1)$$

where  $F_2^p$  and  $F_2^n$  are the proton and neutron structure functions. Under isospin symmetry,  $I_G$  can be expressed in terms of parton distribution functions as:

$$I_G = \frac{1}{3} \int_0^1 [u_v(x, Q^2) - d_v(x, Q^2)] dx + \frac{2}{3} \int_0^1 [\bar{u}_s(x, Q^2) - \bar{d}_s(x, Q^2)] dx \quad (2)$$

If we assume flavor symmetry in the nucleon sea ( $\bar{u}(x) = \bar{d}(x)$ ),  $I_G$  would be equal to 1/3. Measurements by the New Muon Collaboration (NMC) [13] determined that  $I_G = \int_{0.004}^{0.8} [F_2^p(x, Q^2) - F_2^n(x, Q^2)] \frac{dx}{x} = 0.221 \pm 0.021$  at  $Q^2 = 4$  (GeV/c)<sup>2</sup>. Extrapolation to  $x=0$  through the unmeasured small- $x$  region, they projected that  $I_G = 0.235 \pm 0.026$ , significantly below  $\frac{1}{3}$ . Specially, the NMC results indicated that  $\int_0^1 [\bar{d}(x) - \bar{u}(x)] dx = 0.148 \pm 0.039$ .

The second piece evidence is from the Drell-Yan (DY) process. At Fermilab, with 800 GeV/c proton beam, E866 collaboration reported measurements of the

---

<sup>1</sup>The NLO QCD corrections are being studied [10] and results are expected before the running of the proposed experiment

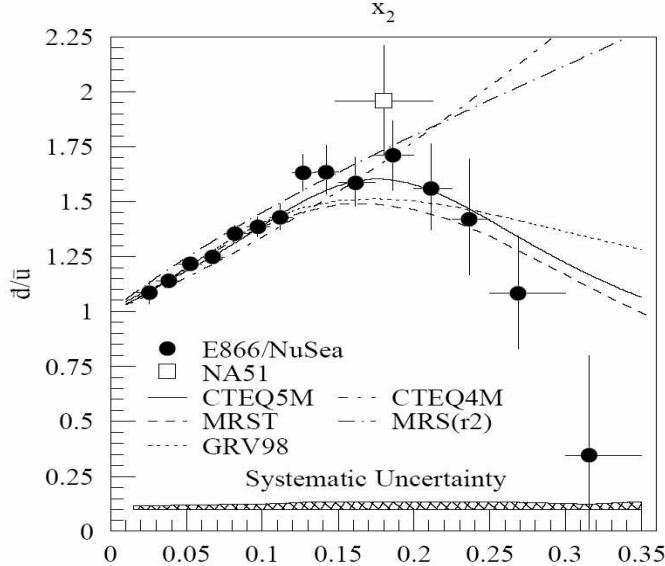


Figure 1: Fermilab E866 results. The ratio of  $\bar{d}/\bar{u}$  is shown as a function of  $x$ . The result from CERN experiment NA51 is shown as an open square.

yield ratio of the Drell-Yan muon pairs production on hydrogen and deuterium target [4]. Under isospin symmetry, the yield ratio of pd and pp can be related to the  $\bar{d}/\bar{u}$ . Assuming isospin symmetry, the Drell-Yan ratio can be expressed as:

$$\frac{\sigma^{pd}}{2\sigma^{pp}} \approx \frac{1}{2}(1 + \frac{\bar{d}_2}{\bar{u}_2}) \quad (3)$$

where the subscript 2 indicates the beam quark (1 would be for target quark). The data suggest that the light quark is flavor asymmetric in the nucleon sea (Fig. 1).

The third piece of evidence is from the SIDIS process. HERMES collaboration reported the  $\bar{d}(x) - \bar{u}(x)$  results (Fig. 2) with a 27.5 GeV positron beam on hydrogen and deuterium target [3]. Although the experiment was performed at a much smaller  $Q^2$  value with a completely different physical process from the Drell-Yan process, the HERMES results on the nucleon sea quark flavor asymmetry are consistent with the E866 data. However, the experimental uncertainty is quite large for the HERMES data, and more precise measurements are needed for further study. The consistency between precise SIDIS measurements and measurements from other hard scattering processes (inclusive, Drell-Yan, etc) can provide important support for the validity of using SIDIS process which is still at an early stage in the study of the nucleon structure, for example the transversity distributions.

Many theoretical models including meson cloud model, chiral-quark model, Pauli-blocking model, instanton model, have been proposed to explain the nucleon sea flavor asymmetry. For recent review, see [14, 15, 16]. These models can describe the  $\bar{d}(x) - \bar{u}(x)$  data very well. However, they all have difficulties in explaining the  $\bar{d}/\bar{u}$  data at large  $x$  ( $x > 0.2$ ). The perturbative process gives a symmetric sea for  $u$  and  $d$ , while a non-perturbative process has to give an asymmetric sea. The relative strength of these two processes is reflected in the  $\bar{d}/\bar{u}$  ratio. Unfortunately, due to the limited statistics, the uncertainty of the E866 data is larger in this region.

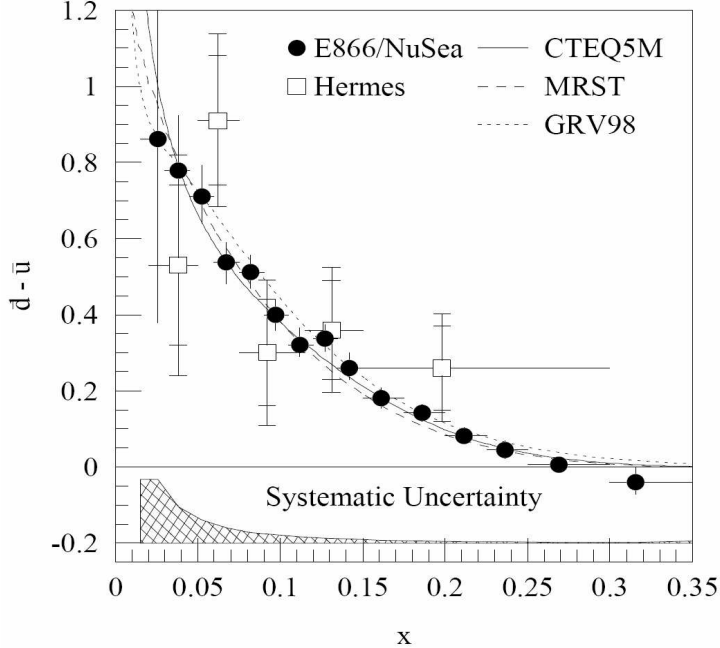


Figure 2: HERMES results,  $\bar{d}(x) - \bar{u}(x)$  as a function of  $x$  at  $Q^2 = 2.3$  ( $\text{GeV}/c$ ) $^2$ . The open circles represent the E866 results at  $Q^2 = 54.0$  ( $\text{GeV}/c$ ) $^2$ .

Therefore, improved measurements of the SIDIS process to confirm this flavor asymmetry is very important. In addition, carrying out precision measurements at lower  $Q^2$  values can also help to constrain the  $Q^2$  dependence of the parton distribution functions by comparing the data from this experiment with the high  $Q^2$  E866 data.

## 2.2 Factorization in parton models

The existence of factorization theorems in QCD implies the universality of the quark and gluon distribution and fragmentation functions in hard scattering processes and their scale dependence. A recent review of the proof of factorization theorem for hard processes in QCD can be found in [17]. While the factorization theorem for integrated  $P_{hT}$  has been established [6], the general factorization theorem for fixed hadron transverse momenta  $P_{hT}$  for SIDIS process has not been proved. A recent development [18] proves the QCD factorization for SIDIS processes at low hadron transverse momenta ( $P_{hT} \ll Q$ ). This new development introduces the transverse-momentum dependent (TMD) parton distributions and fragmentation functions. Here the TMD can be related to the normal Feynman parton distribution function by performing an integration over the transverse momentum. The differential cross-section of SIDIS can be factorized into a product of a TMD parton distribution function, a fragmentation function, a hard scattering part which can be calculated using pQCD and a soft part which can be calculated for  $P_{hT} >> \Lambda_{QCD}$ . In the proposed experiment while  $P_{hT}^2$  is much smaller than  $Q^2$ , the condition that  $P_{hT} >> \Lambda_{QCD}$  is not satisfied. On the high  $P_{hT}$  end, the QCD factorization theorem has been proved for the Drell-Yan process which can be seen as the time-reversal process of SIDIS [19]. It is expected that similar factorization theorem at high  $P_{hT}$  for SIDIS

process can be demonstrated in the near future.

On the other hand, the factorization of SIDIS where the SIDIS process can be factorized into a parton distribution function, a hard scattering part and a fragmentation part is a natural consequence of parton model. In this case, the cross section can be written as a convolution integral of parton distributions and fragmentation functions. The SIDIS processes have been used by a number of collaborations (SMC, HERMES, etc) to extract parton or fragmentation information. The data of SMC and HERMES support the LO  $x - z$  factorization, implying that the spin-independent ( $\sigma_h$ ) hadron production cross-sections factorize into the  $x$ -dependent quark-distributions and the  $z$ -dependent quark fragmentation functions. Meanwhile, the formalism of factorization within parton model has been established [7, 20]. In this proposal, our approach to extract light sea quark flavor asymmetry is based on the factorization assumption of the parton model. In addition, assumptions of transverse momentum dependence of parton distribution function and fragmentation functions are made to achieve the  $x - z$  factorization in the LO analysis. In the next section, our formula of NLO SIDIS cross section is also based on these transverse momentum assumptions.

### 2.3 SIDIS cross section at leading order and the next-to-leading order

Semi-inclusive reactions in electron scattering can be used as a powerful tool to study distribution of the valence quarks as well as that of the sea quarks. With the factorization assumption of SIDIS, at the leading order of  $\alpha_s$ , the SIDIS process is factorized into a hard quark scattering followed by a quark hadronization process, as shown in the first diagram at Fig. 3. The unpolarized cross section can be written as [21]:

$$\frac{d\sigma^h}{dxdydzd^2\mathbf{P}_{\mathbf{hT}}} = \frac{4\pi\alpha^2 s}{Q^4} (1 - y + \frac{y^2}{2}) \sum_q e_q^2 [f_1^q \odot D_1^{qh}] \quad (4)$$

where  $x = Q^2/2M\nu, z = E_h/\nu$ ,  $e_f$  is quark charge,  $f_1^q(x)$  are quark distribution functions of flavor q ( $q = u, \bar{u}, d, \bar{d}, s, \bar{s}$ ). The functions  $D_1^{qh}(z)$  represent the probability that a quark q fragments into a hadron h. The convolution in Eqn.4 represents an integration over transverse momentum of initial ( $k_T$ ) and final quark ( $p_T$ ) with proper weighting [7, 21]:

$$[\dots \odot \dots] = \int d^2 p_T d^2 k_T \delta^{(2)}(\mathbf{p}_T - \frac{\mathbf{P}_{\mathbf{hT}}}{z} - \mathbf{k}_T) [\dots]. \quad (5)$$

In order to perform the integral in Eqn.5, certain assumptions of the transverse momentum dependence of parton distribution function and fragmentation function has to be made. One common assumption of the transverse momentum dependence is a Gaussian shape:

$$f_1^q(x, k_T^2) = f_1^q(x) \frac{1}{\pi\mu_0^2} \exp(-\frac{k_T^2}{\mu_0^2}) \quad (6)$$

$$D_1^{qh}(z, q_T^2) = D_1^{qh}(z) \frac{1}{\pi\mu_D^2} \exp(-\frac{q_T^2}{\mu_D^2}) \quad (7)$$

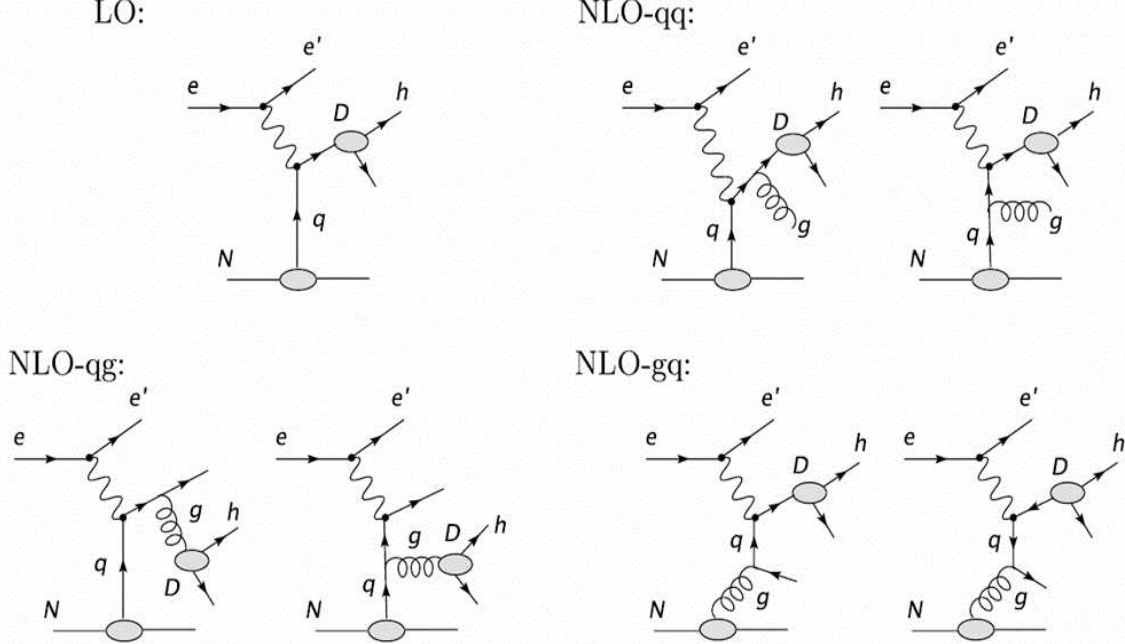


Figure 3: Semi-inclusive deep inelastic scattering diagrams at leading order (LO) and the next-to-leading order (NLO).

where the  $k_T$  is transverse momentum of quark,  $q_T$  is transverse momentum of leading hadron,  $\mu_0^2$  is the average quark transverse momentum square ( $\mu_0^2 = \langle k_T^2 \rangle \approx 0.25(\text{GeV}/c)^2$ ) and  $\mu_D^2$  is the average leading hadron transverse momentum square ( $\mu_D^2 = \langle P_{hT}^2 \rangle \approx 0.2(\text{GeV}/c)^2$ ). Then Eqn.4 can be simplified by performing the integration:

$$\sigma^h(x, z) \sim \sum_i e_f^2 f_1^q(x) \cdot D_1^{qh}(z) \quad (8)$$

The naive  $x$ - $z$  factorization (LO  $x - z$  factorization) is violated at the next-to-leading order when the one-gluon diagrams in Fig. 3 are considered. However, the exact form of this violation are well-known [20]. At NLO, the terms of  $q(x) \cdot D(z)$  ( $q(x)$  instead of  $f_1^q(x)$ ) in Eqn.8 are added with the double convolutions of the type  $q \otimes C \otimes D$  in which  $C$  are well known Wilson coefficients [22]:

$$[q \otimes C \otimes D](x, z) = \int_x^1 \frac{dx'}{x'} \int_z^1 \frac{dz'}{z'} q\left(\frac{x}{x'}\right) C(x', z') D\left(\frac{z}{z'}\right) \quad (9)$$

Not only are  $x$  and  $z$  mixed through the double convolutions at the next-to-leading order, the unpolarized cross section  $\sigma_h$  also depends on the virtual photon variable  $y = (E_0 - E')/E_0$  due to the longitudinal component of the virtual photon and other higher twist effects. Here, we only present leading-twist result of cross section due to the transverse component of the virtual photon.

We define the short-hand notation:

$$qD + \frac{\alpha_s}{2\pi} q \otimes C \otimes D = q[1 + \otimes \frac{\alpha_s}{2\pi} C \otimes]D, \quad (10)$$

at NLO instead of Eqn.8, we have:

$$\begin{aligned}\sigma^h(x, z) = & \sum_f e_f^2 f_1^{qf} [1 + \otimes \frac{\alpha_s}{2\pi} C_{qq} \otimes] D_1^{qh} \\ & + (\sum_f e_f^2 q_f) \otimes \frac{\alpha_s}{2\pi} C_{gq} \otimes D_1^{Gh} + G \otimes \frac{\alpha_s}{2\pi} C_{gq} \otimes (\sum_f e_f^2 D_1^{qh}).\end{aligned}\quad (11)$$

For any given form of the parton distributions, the SIDIS cross sections can be calculated numerically according to Eqn.11. Based on this formalism, the NLO QCD correction can be performed in extracting the parton distributions.

## 2.4 Sea quark flavor asymmetry extraction: leading-order method I

Under the LO  $x - z$  factorization assumption, the semi-inclusive pion production yield at leading twist can be expressed as:

$$Y^{\pi^\pm}(x, z) \propto \sum_i e_i^2 [q_i(x) D_{qi}^{\pi^\pm}(z) + \bar{q}_i(x) D_{\bar{q}i}^{\pi^\pm}(z)] \quad (12)$$

With isospin symmetry, the anti-quark asymmetry can be determined:

$$r_h = \frac{\bar{d}(x) - \bar{u}(x)}{u(x) - d(x)} = \frac{J(z) - \frac{1+r(x,z)}{1-r(x,z)}}{J(z) + \frac{1+r(x,z)}{1-r(x,z)}} \quad (13)$$

where

$$r(x, z) = \frac{Y_p^{\pi^-}(x, z) - Y_n^{\pi^-}(x, z)}{Y_p^{\pi^+}(x, z) - Y_n^{\pi^+}(x, z)}, \quad (14)$$

$$Y_n^\pi = Y_d^\pi - Y_p^\pi \quad (15)$$

and

$$J(z) = \frac{3}{5} \left( \frac{1 + D'(z)}{1 - D'(z)} \right) \quad (16)$$

Here the  $D'(z)$  is defined as  $D_u^-/D_u^+$ , where under isospin symmetry and charge conjugation invariance:

$$D^+ \equiv D_u^{\pi^+} = D_d^{\pi^+} = D_{\bar{u}}^{\pi^+} = D_{\bar{d}}^{\pi^+} \quad (17)$$

and

$$D^- \equiv D_u^{\pi^-} = D_d^{\pi^-} = D_{\bar{u}}^{\pi^-} = D_{\bar{d}}^{\pi^-} \quad (18)$$

are the favored and unfavored light quark fragmentation functions, respectively. In experiments, by neglecting the strange quark contribution, we can measure  $D'(z)$  through the deuterium yields as:

$$D'(z) = \frac{AY_d^{\pi^-} - Y_d^{\pi^+}}{AY_d^{\pi^+} - Y_d^{\pi^-}} \quad (19)$$

where

$$A = \frac{4 + \frac{\bar{u} + \bar{d}}{u + d}}{1 + 4 \frac{\bar{u} + \bar{d}}{u + d}}. \quad (20)$$

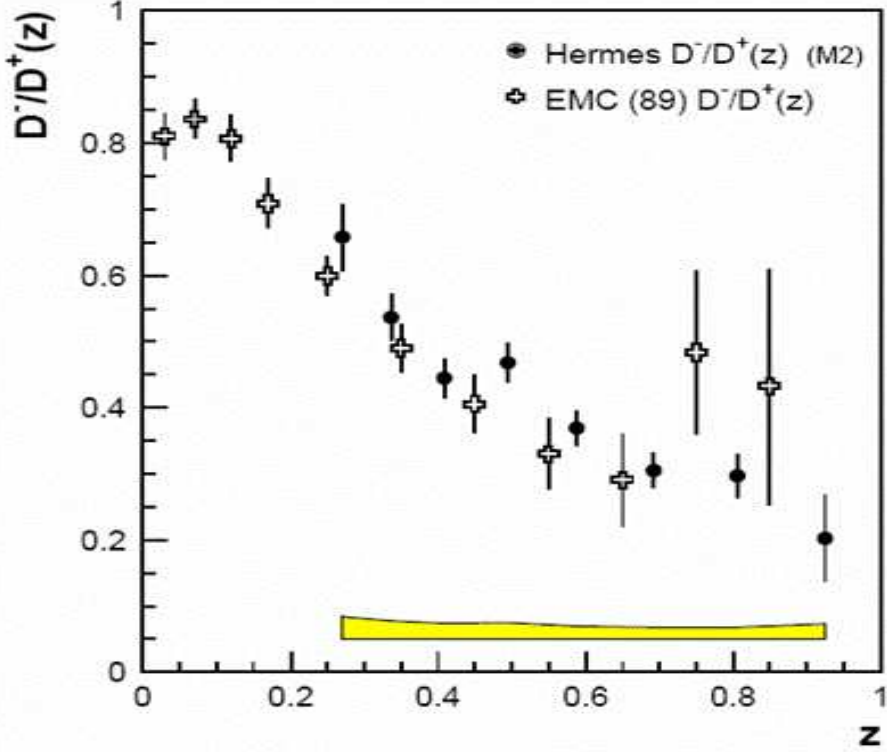


Figure 4: Comparison of favored and unfavored fragmentation function ratio between HERMES and SMC.

Here parton distribution function input  $\frac{\bar{u}+\bar{d}}{u+d}$  are needed. A measurement of  $D'(z)$  at high  $x$  region can minimize the contribution of sea quark along with its systematic uncertainties. The  $D'(z)$  was extracted [3] from semi-inclusive charged pion production from hydrogen, deuterium, using leading order parton distribution functions [23]. Their results from different targets are consistent with each other within statistical errors. In addition, the comparison of HERMES extracted  $D'(z)$  ( $Q^2 = 2.3(\text{GeV}/c)^2$ ) and SMC extracted  $D'(z)$  ( $Q^2 = 25.0(\text{GeV}/c)^2$ ) show a weak  $Q^2$  dependence of  $D'(z)$  (Fig. 4). In addition, the NLO  $Q^2$  evolution has been developed for the fragmentation function [24]. We will carry out a global fit by combining our proposed measurement of  $D'(z)$  with the world data on this quantity.

In this method, a non-zero  $r_h$  would serve as direct evidence for an asymmetric sea-quark distribution. We can obtain  $\bar{d}(x) - \bar{u}(x)$  and  $\bar{d}(x)/\bar{u}(x)$  using the parton distribution function inputs  $(u - d)(x)$  and  $(\bar{d} + \bar{u})(x)$ .

$$\bar{d}(x) - \bar{u}(x) = r_h \cdot (u - d)(x) \quad (21)$$

and

$$\frac{\bar{d}(x)}{\bar{u}(x)} = \frac{(\bar{d}(x) - \bar{u}(x)) + (\bar{d}(x) + \bar{u}(x))}{-(\bar{d}(x) - \bar{u}(x)) + (\bar{d}(x) + \bar{u}(x))} \quad (22)$$

## 2.5 Sea quark flavor asymmetry extraction: leading-order method II

With the LO  $x - z$  factorization assumption, the semi-inclusive pion production yield at leading twist can be expressed as:

$$Y^{\pi^\pm}(x, z) \propto \sum_i e_i^2 [q_i(x) D_{q_i}^{\pi^\pm}(z) + \bar{q}_i(x) D_{\bar{q}_i}^{\pi^\pm}(z)] \quad (23)$$

With the isospin symmetry and neglecting heavy quark contributions, ratios of yields can be formed in which the fragmentation functions cancel each other:

$$t_1(x) = \frac{Y_p^{\pi^+} + Y_p^{\pi^-}}{Y_n^{\pi^+} + Y_n^{\pi^-}} = \frac{4u(x) + d(x) + 4\bar{u}(x) + \bar{d}(x)}{4d(x) + u(x) + 4\bar{d}(x) + \bar{u}(x)} \quad (24)$$

$$t_2(x) = \frac{Y_p^{\pi^+} - Y_p^{\pi^-}}{Y_n^{\pi^+} - Y_n^{\pi^-}} = \frac{4u(x) - d(x) - 4\bar{u}(x) + \bar{d}(x)}{4d(x) - u(x) - 4\bar{d}(x) + \bar{u}(x)} \quad (25)$$

Or simply as:

$$r_1(x) = \frac{4 - t_1(x)}{4t_1(x) - 1} = \frac{d(x) + \bar{d}(x)}{u(x) + \bar{u}(x)} = \frac{d_v(x) + 2\bar{d}(x)}{u_v(x) + 2\bar{u}(x)} \quad (26)$$

and

$$r_2(x) = \frac{4 + t_2(x)}{4t_2(x) + 1} = \frac{d(x) - \bar{d}(x)}{u(x) - \bar{u}(x)} = \frac{d_v(x)}{u_v(x)} \quad (27)$$

in which  $u_v(x) = u(x) - \bar{u}(x)$  and  $d_v(x) = d(x) - \bar{d}(x)$ .

In the above formalism, the  $Q^2$  dependent fragmentation function will be canceled exactly. Clearly, the observation of  $r_1 \neq r_2$  would serve as direct evidence for a non-vanishing sea-quark distribution. Furthermore, a precise measurement of  $r_1$  and  $r_2$  at different  $x$  and  $Q^2$  will provide strong and independent constraints on the parton distribution functions, especially in high- $x$  region where existing data lack accuracy. With the parton distribution function inputs  $(u + \bar{u})(x)$  and  $(\bar{u} + \bar{d})(x)$ , we can form different sea flavor asymmetry variables:

$$(\bar{d} - \bar{u})(x) = \frac{(r_2 - 1)(\bar{u} + \bar{d})(x) - (r_2 - r_1)(u + \bar{u})(x)}{r_2 + 1} \quad (28)$$

and

$$\frac{\bar{d}}{\bar{u}}(x) = \frac{2(\bar{d} + \bar{u})(x)r_2 - (u + \bar{u})(x)(r_2 - r_1)}{(u + \bar{u})(x)(r_2 - r_1) + 2(\bar{d} + \bar{u})(x)}. \quad (29)$$

Both Method I and Method II will be used to analyze the same data set providing cross-check. Compared with Method I, Method II has two advantages.

- The fragmentation functions are canceled in forming yield ratios  $r_1$  and  $r_2$ . Only the parton distribution function information is needed in extracting different sea flavor asymmetry variables.
- The  $r_2 = d_v/u_v$  behaves as a flavor non-singlet quantities. In NLO,  $r_2$  can be expressed as:

$$r_2 = \frac{d_v[1 + \otimes(\alpha_s/2\pi)C_{qq}](D^+ - D^-)}{u_v[1 + \otimes(\alpha_s/2\pi)C_{qq}](D^+ - D^-)} \quad (30)$$

From the above equation, it can be seen clearly that  $r_2$  does not mixed with gluon distribution and gluon fragmentation. Therefore,  $r_2$  is one of the cleanest quantities in the NLO QCD analysis.

## 2.6 NLO QCD correction and NLO global fits

The formalism of SIDIS cross-section including the next-to-leading order contributions has been well established. Several global fitting efforts on asymmetries have been carried out in recent years when SIDIS data became available [25, 26], though such fitting procedures have not been tried on the cross-section data yet. The NLO global fitting procedures of SIDIS data follows the similar strategy as in the NLO inclusive DIS fitting. When the data of this experiment become available, analysis including the NLO QCD corrections can be performed in addition to the two leading-order methods. Meanwhile, we expect that a global fitting procedure will be carried out by theorists [10].

## 2.7 Charged kaon production in SIDIS

With the excellent kaon detection capability, kaons will be detected parasitically during this experiment. By the same convention, the kaon fragmentation functions are grouped into three different types:

$$D_K^+ \equiv D_u^{K^+} = D_{\bar{u}}^{K^-} = D_s^{K^+} = D_{\bar{s}}^{K^-}, \quad (31)$$

$$D_K^- \equiv D_{\bar{u}}^{K^+} = D_u^{K^-} = D_s^{K^+} = D_{\bar{s}}^{K^-}, \quad (32)$$

$$D_K^d \equiv D_d^{K^+} = D_{\bar{d}}^{K^+} = D_d^{K^-} = D_{\bar{d}}^{K^-}. \quad (33)$$

Here  $D_K^+$  is the favored fragmentation function, while the other two are the unfavored fragmentation functions. Under the assumption of LO  $x - z$  factorization, the yield of SIDIS kaon production can be written as the product of parton distribution function and kaon fragmentation function. Using similar method, we can extract valance quark ratio from kaon yields:

$$t_2^K(x) = \frac{Y_p^{K^+} - Y_p^{K^-}}{Y_n^{K^+} - Y_n^{K^-}} = \frac{u(x) - \bar{u}(x)}{d(x) - \bar{d}(x)} = \frac{u_v(x)}{d_v(x)}. \quad (34)$$

An independent check of the  $u_v(x)/d_v(x)$  ratio can be obtained from the charged kaon SIDIS data. These data also allow a direct test of LO  $x - z$  factorization for kaon production.

It is natural to extend our study to investigate the possible sea flavor asymmetry in the meson system. In the  $\pi^+$  case, the charge-conjugation symmetry and isospin asymmetry indicated that  $\bar{u} = d$  in  $\pi^+$  and Pauli-blocking also suggest this symmetry. Therefore, the sea quark distributions in the charged pions are expected to be u/d symmetric.

The situation is quite different for kaons. In the  $K^+$  case, which is  $u\bar{s}$ . Light quark flavor asymmetry in the kaon sea would imply  $\bar{u} \neq \bar{d}$ . Compared with pion case, there is no requirement for equality of these two sea quark distributions. One also anticipates such an asymmetry from the Pauli-blocking picture where  $u$  quark is one of the valence quarks. Although the connection between the parton distribution

function and the fragmentation function is still unclear, one possible candidate which may access this asymmetry is by measuring the kaon flavor fragmentation function asymmetry. A possible evidence for such an asymmetry already exists. Kaon fragmentation functions have been extracted by Kniehl *et al.* [27] by fitted the hadron production data from  $e^+e^-$  annihilation. They obtain the following surprising result ( $Q_0^2=2$  (GeV/c) $^2$ ):

$$\int_{0.05}^1 z D_{u,s}^{K^\pm}(z, Q_0^2) dz = 0.057 \quad (35)$$

$$\int_{0.05}^1 z D_d^{K^\pm}(z, Q_0^2) dz = 0.25 \quad (36)$$

where

$$D_{u,s}^{K^\pm} = \frac{1}{2}(D_u^{K^\pm} + D_{\bar{u}}^{K^\pm} + D_s^{K^\pm} + D_{\bar{s}}^{K^\pm}) = (D_u^{K^+} + D_{\bar{u}}^{K^+}) \quad (37)$$

and

$$D_d^{K^\pm} = (D_d^{K^\pm} + D_{\bar{d}}^{K^\pm}) = 2D_{\bar{d}}^{K^+} \quad (38)$$

Then we can easily see that

$$\int_{0.05}^1 2z(D_u^{K^+} + D_{\bar{u}}^{K^+}) dz = 0.114 < 0.25 = \int_{0.05}^1 2zD_{\bar{d}}^{K^+} dz \quad (39)$$

which means

$$\int_{0.05}^1 z D_{\bar{u}}^{K^+} dz < \int_{0.05}^1 z D_{\bar{d}}^{K^+} dz \quad (40)$$

This results shows that the  $\bar{d}$  quark, which is a sea quark for  $K^+$ , has a much higher probability to fragment into a  $K^+$  than for the  $\bar{u}$  sea quark. We propose to measure the following quantity neglecting the strange quark contribution:

$$\frac{D_d^{K^\pm}}{D_u^{K^\pm}} \equiv \frac{2D_{\bar{d}}^{K^+}}{D_K^+ + D_K^-} \approx 4 \frac{(Y_n^{K^+} + Y_n^{K^-}) - r_1(Y_p^{K^+} + Y_p^{K^-})}{(Y_p^{K^+} + Y_p^{K^-}) - r_1(Y_n^{K^+} + Y_n^{K^-})} \quad (41)$$

where

$$r_1 = \frac{d(x) + \bar{d}(x)}{u(x) + \bar{u}(x)} \quad (42)$$

The above relation shows that kaon SIDIS may provide information on the possible flavor asymmetry of the kaon fragmentation function. Such measurements (SIDIS) have never been carried out before.

## 2.8 Indications of leading order $x - z$ factorization by existing data

From the previous discussion, the factorization assumption (LO  $x - z$  factorization) within parton model is very important to our analysis (LO analysis) of SIDIS process. So it is very crucial to test the validity of the LO  $x - z$  factorization assumption at relatively low  $Q^2$  regime ( $Q^2 \approx 1 - 4.5$  (GeV/c) $^2$ ) by experiments. Evidence supporting the LO  $x - z$  factorization assumption have been reported for this  $Q^2$  range. The HERMES [3] Collaboration reported earlier evidence for the  $z$  independence

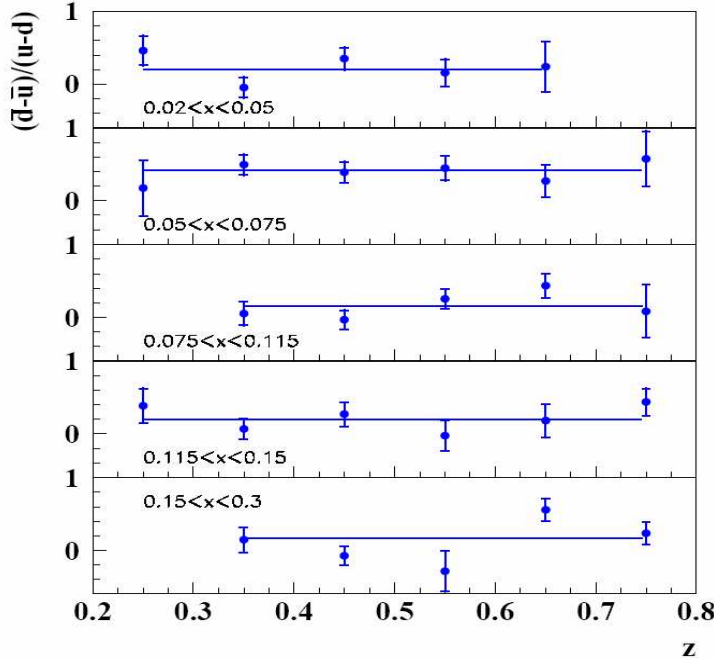


Figure 5: HERMES evidence of factorization. The distribution of  $(\bar{d} - \bar{u})/(u - d)$  as a function of  $z$  in five bins of  $x$ .

within the experimental uncertainty in the range of  $0.3 < z < 0.8$  in the measured ratio of  $(\bar{d} - \bar{u})/(u - d)$  (Fig. 5)<sup>2</sup>. JLab Hall C E00-108 [8] experiment studies quark-hadron duality and tests the low energy LO  $x - z$  factorization assumption through meson electro-production. Preliminary results [28] (Fig. 6) show that the data are consistent with  $x - z$  factorization in the region of  $0.35 < z < 0.65$ . Recently, the JLab CLAS collaboration [9] reported the first evidence for a non-zero beam-spin azimuthal asymmetry in the semi-inclusive production of positive pions in the DIS region. Furthermore, the study of the pion multiplicities as a function of  $x$  has been carried out and no  $x$  dependence has been observed, and this finding is consistent with the assumption of the LO  $x - z$  factorization. Therefor, we assume a LO  $x - z$  factorization for our LO QCD analysis (Method I and Method II) for a  $z$  range of  $0.35 < z < 0.65$ .

With an incident electron beam energy up to 11 GeV, Jefferson Lab has unique advantages to carry out a measurement of semi-inclusive hadron yields from deep-inelastic scattering: fixed targets allow for a significantly higher luminosity compared with that of the HERMES experiment, the kinematics allow for a probe of the interesting high  $x$  region, where the asymmetry is poorly known. A precision determination of the asymmetry at high  $x$  will provide stringent constraints on nucleon structure models, which give rise to rather different predictions for the  $x > 0.3$  [29, 30] region.

---

<sup>2</sup>Later analysis seem to suggest that the  $z$ -independent observation may not be conclusive.

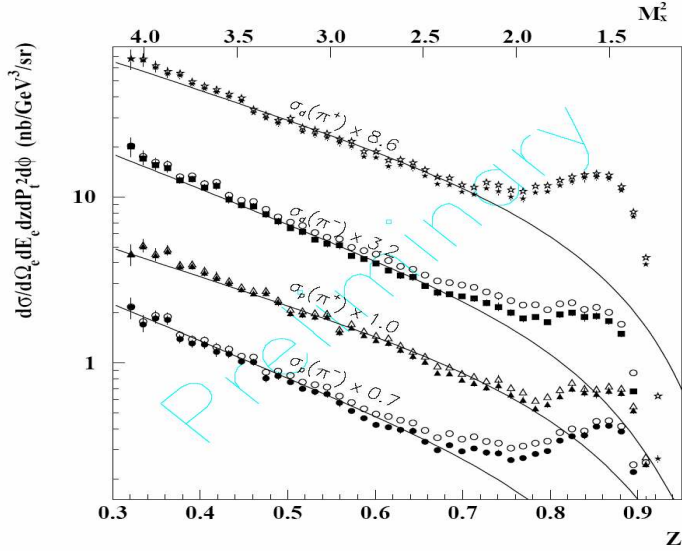


Figure 6: Preliminary E00-108 semi-inclusive  $\pi^\pm$  production cross-sections on hydrogen and deuterium target (points) at  $x = 0.32$  as a function of  $z$  in comparison with a Monte Carlo simulation (solid curve) starting from a factorization and fragmentation ansatz. The difference between the open symbols and solid symbols corresponds to exclusive  $\rho$  production.

### 3 Experiment

#### 3.1 Experimental overview

We proposed to study the nucleon sea flavor asymmetry using the SIDIS process at Jefferson Lab in Hall C with a 11 GeV electron beam. We plan to measure the SIDIS ( $e, e'\pi^\pm$ ) and ( $e, e'K^\pm$ ) yields from the standard 15 cm long hydrogen and deuterium targets with high statistical accuracy. With these four  $\pi$  yields, we will extract the yield ratios  $r_1$ ,  $r_2$ ,  $r_h$  and  $D'(z)$  to high statistical precision in order to extract the  $x$ -dependence of the light anti-quark distribution ratio ( $\bar{d}/\bar{u}$ ).

The proposed Super High Momentum Spectrometer (SHMS) will be positioned far forward to detect the scattered electrons. In order to cover a large range of  $Q^2$  and Bjorken  $x$ , the SHMS will be positioned at  $9.1^\circ$ ,  $11.0^\circ$  and  $13.0^\circ$ . A gas Čerenkov detector and Lead-glass shower counters can provide an excellent particle identification (PID). The hadron arm will be the Hall-C HMS spectrometer positioned at  $-11.8^\circ$ ,  $-14.5^\circ$  and  $-15.2^\circ$  (to the beam left when facing the beam dump). A heavy gas Čerenkov detector, shower counter together with one aerogel Čerenkov detector ( $n=1.015$  or  $n=1.03$  depending momentum setting) can provide excellent particle identification (PID) of pions and kaons over a wide momentum range. With the excellent kaon PID, we will be able to study the kaon flavor dependent fragmentation functions which are poorly known.

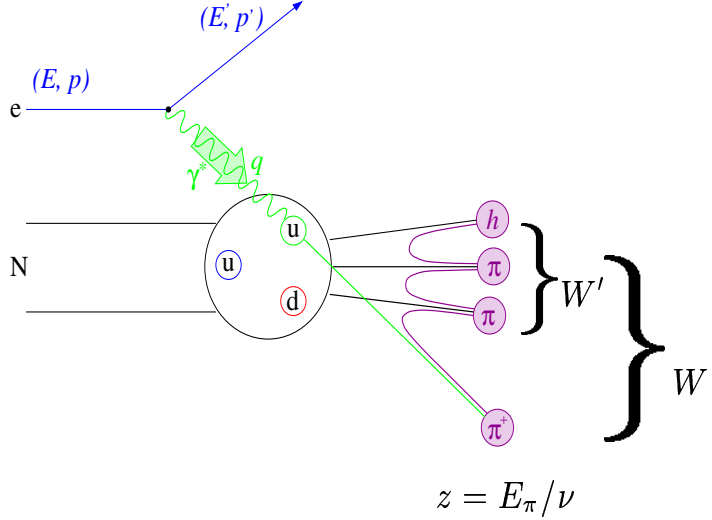


Figure 7: Diagram of  $(e, e' \pi)$  reaction on nucleon.

### 3.2 Choice of kinematics

The definitions of the kinematic variables are the following (Fig. 7): Bjorken- $x$ , which indicates the fractional momentum carried by the struck quark, is  $x = Q^2/(2\nu M_N)$ , where  $M_N$  is the nucleon mass. The momentum of the outgoing hadron is  $P_h$  and the fraction of the virtual photon energy carried by the hadron is:  $z = E_h/\nu$ .  $W$  is the invariant mass of the whole hadron system and  $W'$  is the invariant mass of the hadron system without the detected hadron. We have:

$$W^2 = M_N^2 + Q^2 \left( \frac{1}{x} - 1 \right), \\ W'^2 = (M_N + \nu - E_\pi)^2 - |\vec{q} - \vec{p}_\pi|^2 \quad (43)$$

In order to ensure this experiment is in the DIS region, we chose high  $Q^2$ ,  $W$  and  $W'$ . Meanwhile, in order to test the factorization assumption, we chose to cover a relative large  $Q^2$  and  $z$  range,  $2.3 < W < 3.2$  GeV,  $0.11 < x < 0.5$ ,  $1.2 < Q^2 < 4.3$  ( $GeV/c$ ) $^2$  and  $0.3 < z < 0.7$ . We also choose to spend 70% of our time in detecting the leading fragmentation pion which carries  $z \approx 0.47$  of the energy transfer to favor current fragmentation. The value of  $W'$  is also chosen to be as high as possible<sup>1</sup> with a cut of  $W' > 1.6$  GeV to avoid contributions from resonance production channels. There will be three momentum and angle settings for SHMS (electron arm) in order to cover a large  $Q^2$  and  $x$ . Each of them will have three HMS momentum settings to a large  $z$  coverage for LO  $x - z$  factorization test. The kinematics for different settings are listed in Table. 1. We will divide the whole  $x$  range into ten bins. The average  $Q^2$ ,  $z$ ,  $x$ ,  $W$  and  $W'$  for each bin can be found in Table. 2.

In the two-dimensional plot [31] of  $z$  vs  $\eta_{CM}$ , where the center-of-mass rapidity  $\eta_{CM} = \frac{1}{2} \ln \frac{E+P_L}{E-P_L}$  is defined in the center-of-mass frame, as shown in Fig. 8 for  $W=2.5$  GeV, the rapidity gap between the two fragmentation regimes is  $\Delta\eta_{CM} = 3.8$  when  $z > 0.5$  is required. This condition is well above the regularly used Berger's criteria

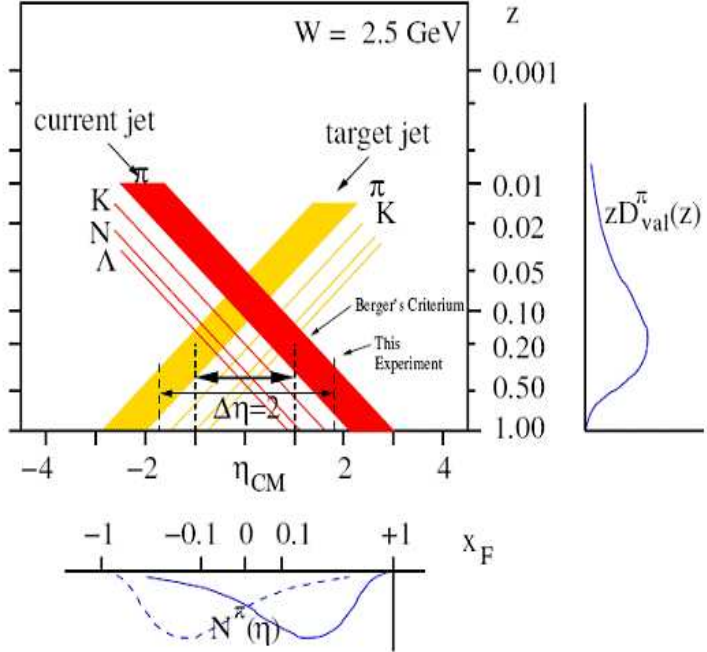


Figure 8: The center-of-mass rapidity gap for  $W = 2.5$  GeV, above  $z=0.5$  the current and target fragmentation regime is separated by  $\Delta\eta_{CM} = 3.8$ . A typical fragmentation function is shown on the side panel with  $z = E_\pi/\nu$  and  $x_F = p_L/|\vec{q}|$ .

of  $\Delta\eta = 2.0$  for separation of current and target fragmentation [32].

The standard 15 cm Hall C cryogenic Hydrogen and Deuterium targets will be used. Target density will be monitored by pressure and temperature measurements. Single arm electron events will also be used for the monitoring of the target density changes.

The phase plot is obtained from Hall C standard SIMC Monte Carlo simulation which includes realistic spectrometer models of SHMS and HMS as well as the target and detector geometries. The coverage in the  $(Q^2, x)$ ,  $(W, x)$ ,  $(W', x)$  and  $(z, x)$  are shown in Fig. 9. The angular coverage of  $\phi_h$  is shown in Fig. 10. From this plot, we can see the azimuthal angular coverage for most  $x$  bins are very good. In the worst case, it is still larger than  $1/3$  of  $2\pi$ . The higher twist azimuthal angular dependent term can be fitted from the data. More discussions can be found in Sec. 3.8. The transverse momentum coverage is in Fig. 11.

$\theta_e$ deg	$p_e$ GeV/c	$\theta_h$ deg	$p_h$ GeV/c	$I_p^+$ $\mu A$	$I_p^-$ $\mu A$	$I_d^+$ $\mu A$	$I_d^-$ $\mu A$
9.1	6.3	11.8	1.8	2.8	6.0	1.4	3.0
9.1	6.3	11.8	2.2	4.9	10.6	2.4	5.3
9.1	6.3	11.8	2.7	9.0	18.8	4.5	9.4
11.0	6.4	14.5	1.8	4.0	9.1	2.0	4.5
11.0	6.4	14.5	2.2	7.6	17.3	3.8	8.6
11.0	6.4	14.5	2.7	15.1	34.2	7.5	17.1
13.0	6.1	15.2	1.8	4.4	10.2	2.2	5.1
13.0	6.1	15.2	2.25	9.4	21.8	4.7	10.9
13.0	6.1	15.2	2.85	22.8	52.2	11.4	26.1

Table 1:  $I_p^\pm$  is the beam current on hydrogen target with positive/negative polarity magnet setting in HMS. The beam current for deuterium target will be half of the hydrogen target in order to keep the luminosity the same.

$x$	$Q^2$ ( $GeV^2/c^2$ )	$z$	$W$ (GeV)	$W'$ (GeV)
0.139	1.43	0.415	3.12	2.43
0.158	1.57	0.431	3.04	2.34
0.180	1.72	0.448	2.96	2.26
0.206	1.92	0.452	2.88	2.19
0.235	2.19	0.458	2.82	2.14
0.264	2.49	0.456	2.79	2.12
0.294	2.83	0.451	2.76	2.10
0.324	3.06	0.459	2.69	2.04
0.353	3.24	0.462	2.61	1.98
0.401	3.54	0.473	2.48	1.87

Table 2:  $Q^2$ ,  $z$ ,  $W$  and  $W'$  for different  $x$  bins.

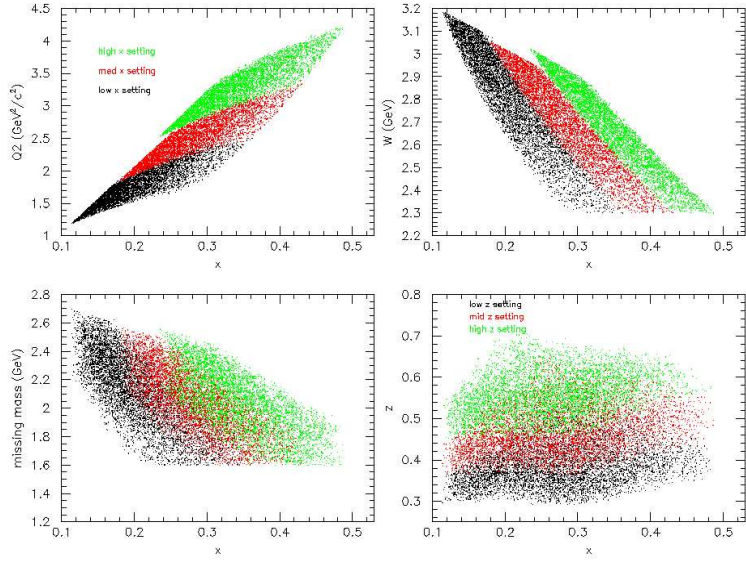


Figure 9: The phase space plots are showed here for different kinematic variables. Three different electron arm settings are presented in different colors. In the  $z$  vs  $x$  plot, three different hadron arm settings are presented in different colors.

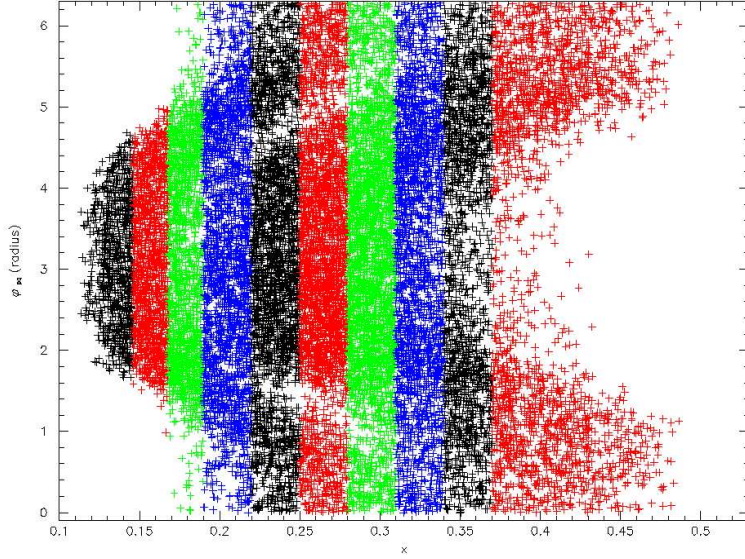


Figure 10: The  $\phi_h$  coverage for different  $x$  bins are shown in this plot. Different colors are used to illustrate different  $x$  bins.

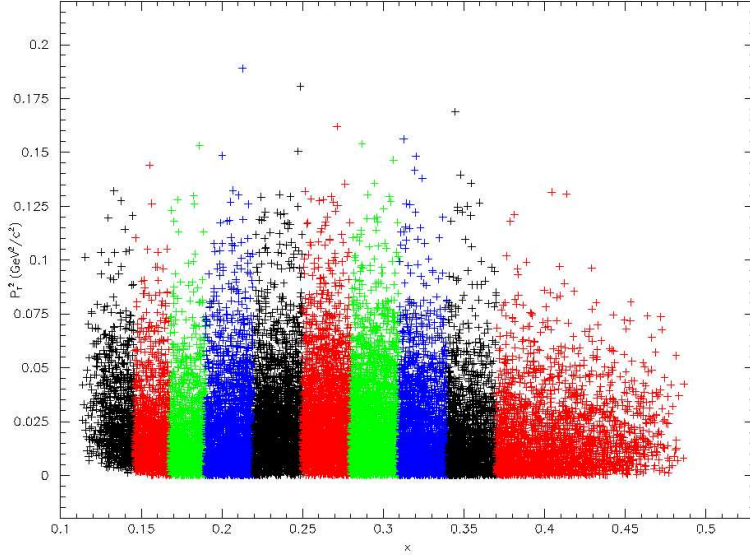


Figure 11: The transverse momentum coverage for different  $x$  bins are shown in this plot. Different colors are used to illustrate different  $x$  bins.

Detector	$P_{min}$ GeV/c	$P_{max}$ GeV/c	$\theta_{cen}^{min}$ degree	$\theta_{cen}^{max}$ degree
HMS	1.62	3.14	11.8	15.2
SHMS	5.19	7.68	9.1	13.0

Table 3:  $Q^2$ ,  $z$ ,  $W$  and  $W'$  for different  $x$  bins.

### 3.3 Spectrometer systems

In this experiment, we will make coincidence measurements between pions (kaons) in HMS and electrons in SHMS (Fig. 12). Similar rates and pion/electron, pion/kaon, pion/kaon/proton separation have been achieved in HALL C for many years in the HMS/SOS combination. For example, the current detector stack of HMS and proposed SHMS will be able to achieve  $e^-/\pi^-$  separation to  $10^4$ . The minimum and maximum momentum and central angle for HMS and SHMS can be seen in Table. 3. For PID, we will combine functions of Time-Of-Flight (TOF), Gas Čerenkov detector, aerogel detector and shower counter. In addition in off-line analysis, we will use coincidence timing between electron arm (SHMS) and hadron arm (HMS). A vertex cut may also be used to reduce backgrounds.

#### 3.3.1 The electron arm: SHMS

The SHMS will be located at forward angle  $9.1^\circ$ ,  $11.0^\circ$ ,  $13.0^\circ$  with momentum setting of 6.3 GeV/c, 6.4 GeV/c and 6.1 GeV/c, respectively. The SHMS acceptance is about 3.8 msr, with  $-15\%$  to  $+20\%$  momentum acceptance. The SHMS will be operated with negative polarity for electron detection. The detector package will be standard electron detecting package which mainly contains a heavy gas Čerenkov,

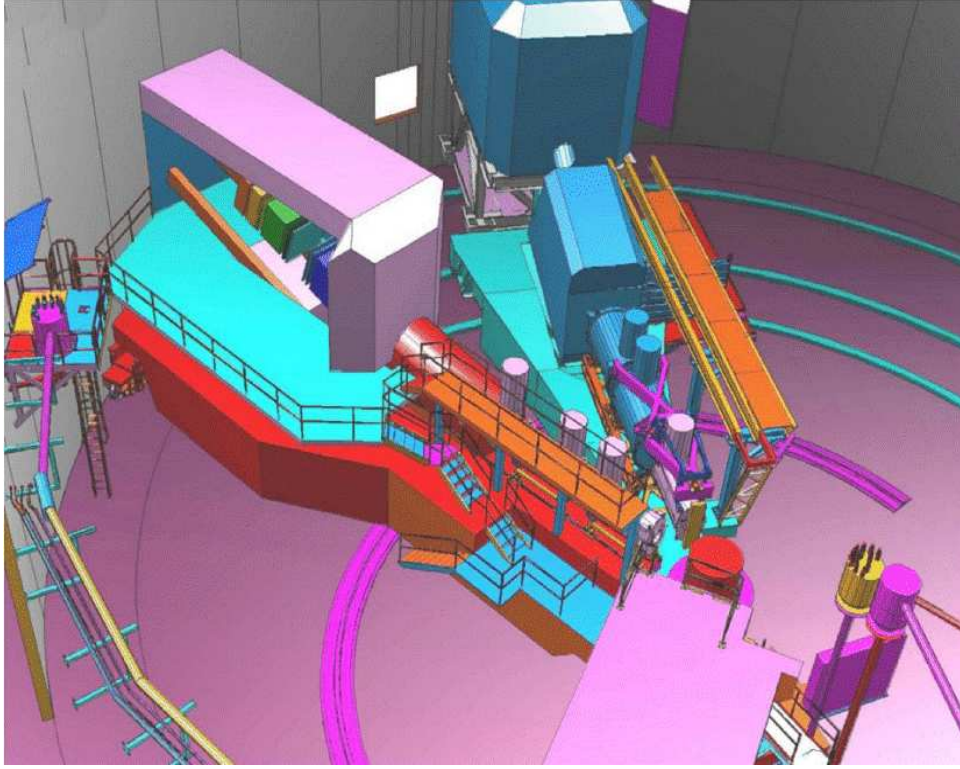


Figure 12: Artist's rendering of SHMS and HMS spectrometers in Hall C.

quartz Čerenkov hodoscope and lead-glass shower counters (Fig. 13).

Shower counter can be used for electron identification by use of energy measurements and electromagnetic shower development in the calorimeter. The resolution of the energy measurement can be estimated by:

$$\frac{\Delta E}{E} \approx \frac{6.1}{\sqrt{E}} + 0.3\% \approx 2.8\%, (6\text{GeV}) \quad (44)$$

The pion rejection factor of 200:1 can be achieved at  $E > 2.0$  GeV with a 99% electron detecting efficiency. It is proposed to construct a threshold Čerenkov using the heavy perfluorocarbon gas  $C_4F_{10}$  as a radiator. Based on the excellent operational experience on similar detector in HMS, we expect that with optimal pressure of gas, we have a clean way for electron identification. The second hodoscope plane

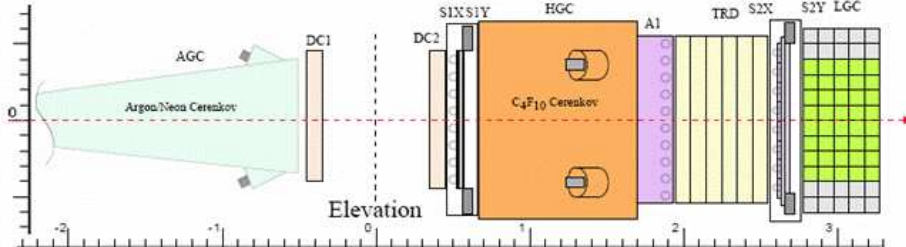


Figure 13: Block Diagram of SHMS Detector Arrangement.

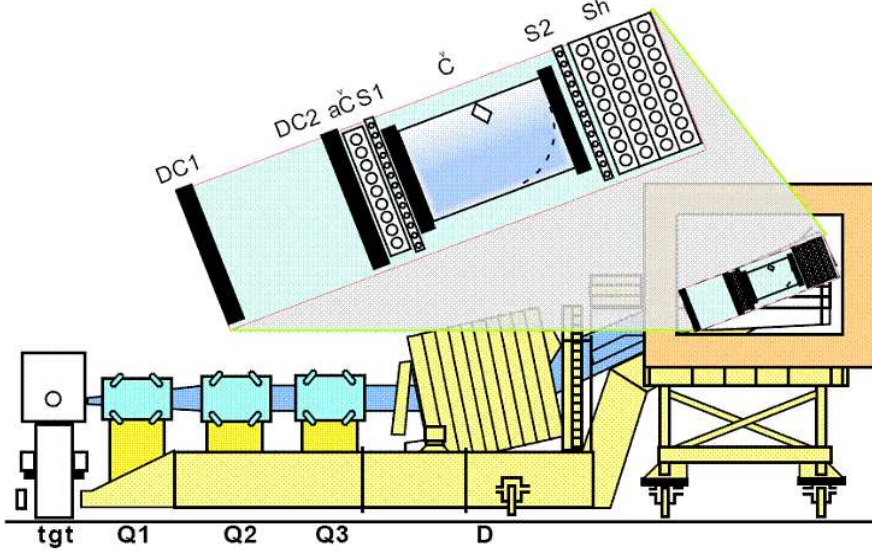


Figure 14: Block Diagram of HMS Spectrometer is shown together with the current detector layout.

in SHMS will consist of a 2-3 cm thick quartz Čerenkov radiator elements. A quartz Čerenkov operated at a threshold of 100 photoelectrons could be essentially 100% efficient and blind to low energy backgrounds, resulting a much cleaner trigger.

Based on all detectors capability, the expected  $e^-/\pi^-$  separation can be achieved to  $10^4 - 10^5 : 1$ . The expected worst case singles  $e^-/\pi^-$  ratio is larger than 2.5. Since we are only interested in coincidence events in this experiment, a cut on the coincidence TOF will further reduce the random  $\pi^-$  contamination to a negligible level.

### 3.3.2 The hadron arm: HMS

The Hall-C HMS (Fig. 14) will serve as the hadron arm spectrometer. The HMS has been used in many experiments which required good particle identification and accurate knowledge of the acceptance. To allow for a significant range in  $z$  for factorization test, three hadron spectrometer magnet settings will be used for each electron arm setting. The HMS acceptance is about 6.4 msr, with a momentum acceptance of  $\pm 10.0\%$ , and positive and negative pions will be detected in separated runs with opposite magnet polarities. The two polarities presenting very different cases for particle identification in HMS. In the positive polarity of HMS we need to separate  $\pi^+$  ( $K^+$ ) from  $p$ ,  $e^+$  and  $K^+$  ( $\pi^+$ ). The main source of  $e^+$  is a pair-symmetric events from decays of photoproduced  $\pi^0$  mesons. As was shown by simulations (Peter Bosted), Hall C measurements (C. Keppel) and tables in Appendix A, the fraction of  $e^+$  is negligible. The ratio of  $p/K^+ \approx 3$  and  $\pi^+/K^+ \approx 8$ . In the case of negative polarity of HMS, we need to separate  $\pi^-$  ( $K^-$ ) from electron and  $K^-$  ( $\pi^-$ ). The ratio of  $e^-/\pi^- \approx 1/40$  and  $K^-/\pi^- \approx 1/20$ .

Shower counter will be used for  $e^-$  ( $e^+$ ) rejection. An 100:1 at 1 GeV/c ( 1000:1 at 2 GeV/c) electron rejection can be achieved with a pion (kaon) detecting efficiency better than 99.5%. Heavy gas Čerenkov will also help in electron pion separation

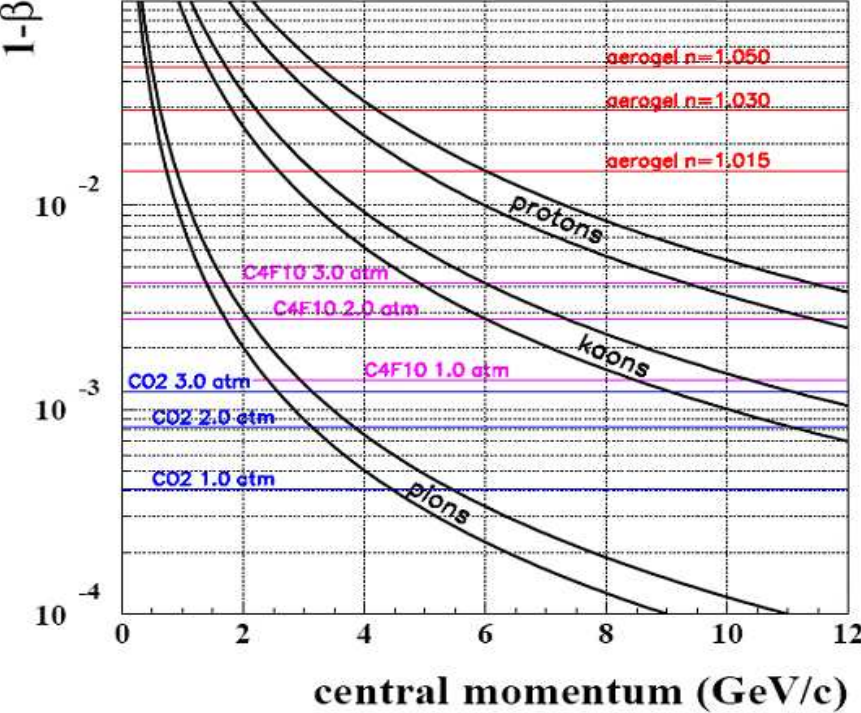


Figure 15: Threshold momentum for pion, K and proton in different Čerenkov detector.

Particle	$P_{threshold}$ GeV/c n=1.03	$P_{threshold}$ GeV/c n=1.015
$\pi$	0.565	0.803
K	2.0	2.840
p	3.802	5.379

Table 4: Threshold momentum for different particles in two aerogel Čerenkov detector.

at low momentum. The total electron rejection is expected to be around 1000 : 1 with detecting efficiency of hadron better than 99.5%. A heavy gas Čerenkov, one aerogel detector ( $n=1.015$  or  $n=1.03$ ) will be used in hadron PID. The threshold momentum for two aerogel Čerenkov detectors with different index can be found in Table. 4. The threshold momentum for different particles in different Čerenkov detector is shown in Fig. 15.

For hadron identification, the following PID strategy will be employed:

- **From 1.6 GeV/c to 2.0 GeV/c (first hadron arm momentum setting)**

Aerogel detector ( $n=1.015$ ) will be installed. Pions will fire aerogel detector. Kaons and protons won't fire the aerogel Čerenkov detector. The relative Time-Of-Flight can be used to separate kaons from protons at this momentum range. A TOF path of 2m with a TOF resolution 200 ps, still allows one to distinguish protons from kaons at the  $3\sigma$  level (300:1 proton rejection) with kaon detection efficiency higher than 99.5%. The heavy gas Čerenkov with 2.5

atm will be used. It will help to exclude electrons and positrons.

- **From 2.0 GeV/c to 2.5 GeV/c (second hadron arm momentum setting)** Aerogel detector ( $n=1.03$ ) will be installed. At this momentum range, both pions and kaons (kaons will start to fire) will fire the  $n=1.030$  aerogel detector, while protons won't fire this aerogel Čerenkov detector. A proton rejection of 1000:1 can be easily achieved in this case. Heavy gas Čerenkov with 2.5 atm (Fig. 15) will be used for  $\pi/K$  separation. Pion will fire the heavy gas Čerenkov detector while kaon won't fire this Čerenkov detector for this momentum range. A pion (kaon) rejection of 1000:1 to kaon (pion) can be achieved.
- **From 2.5 GeV/c to 3.2 GeV/c (third hadron arm momentum setting)** Aerogel detector ( $n=1.03$ ) will be installed. At this momentum range, kaons will definitely trigger  $n=1.03$  aerogel Čerenkov, while protons will not. A good proton rejection can be achieved. The heavy gas Čerenkov with 2.5 atm pressure will be used to do  $\pi/K$  separation. Kaons do not radiate, while pions will radiate. In this case, a pion (kaon) rejection of 1000:1 to kaon (pion) can be achieved.

In summary, full capabilities of the HMS spectrometer in distinguishing protons from pions (kaons) can be achieved to at least 1000:1 (300:1 at first kinematics) with a combination of TOF and aerogel Čerenkov detector. Heavy gas Čerenkov and  $n=1.015$  aerogel Čerenkov can be used to separate pions (kaons) from kaons (pions) to a rejection factor 1000:1. The heavy gas Čerenkov and calorimeter will provide a electron rejection at 1000:1 for pion and kaon detection. In this configuration, the HMS can provide an excellent PID for pion at high efficiency (99%). For kaon detection, a 1000:1 pion rejection together with the TOF cut can provide an excellent kaon detection (about 2000:1 total pion rejection). A detailed PID plots for different particle separation can be seen in Fig. 16.

### 3.4 Trigger, time-of-flight resolution

The electron arm SHMS trigger and the hadron arm trigger in the HMS will be the standard coincidence of 3 out of 4 scintillator planes. PID detector, such as gas Čerenkov detector can be added to the trigger. The coincidence timing resolution is expected to be 200 ps. In this case, a  $\pm 3\sigma$  coincident window (1.2 ns) is assumed.

### 3.5 Target and luminosity normalization

The standard 15 cm Hall C cryogenic Hydrogen and Deuterium targets will be used. The dominant target related systematic errors in the proposed experiment are the proton and deuteron relative luminosity correction and target density fluctuations. With a 50  $\mu\text{A}$  beam and a 15 cm long hydrogen (deuterium) target. The density fluctuation can be a 5% (2.5%) effect. Single arm inclusive data described below will be used to monitor the overall luminosity.

Both methods to extract  $\bar{d} - \bar{u}(x)$  proposed for this experiment rely on precision measurements of  $\pi^+$  and  $\pi^-$  yields on a proton and a deuteron target. However, in both approaches, the equations can be rewritten in terms of multiplicities rather than absolute cross sections, and a term proportional to the inclusive deep inelastic

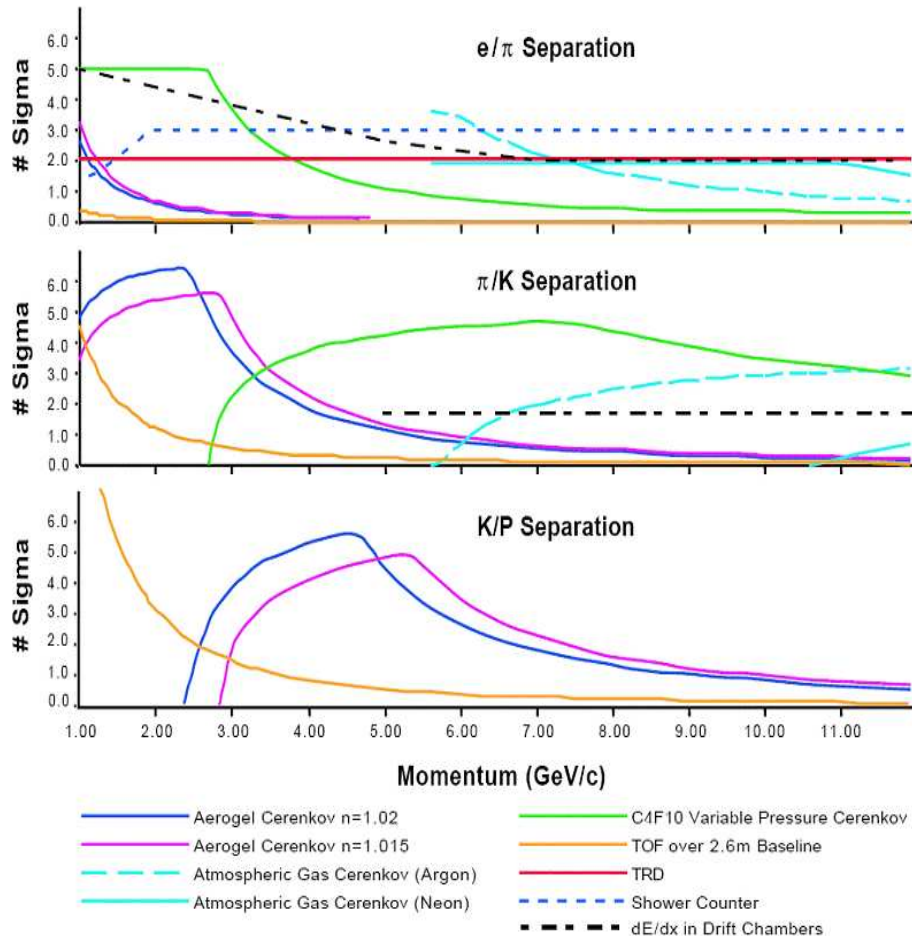


Figure 16: Full capability of PID for different detectors is shown. The vertical scale in each graph is number of standard deviations which separate the two particle types shown, calculated for all of the relevant detectors in the system. Aerogel detector with  $n=1.03$  is not presented here.

cross section ratio of the deuteron and the proton,  $\sigma^d/\sigma^p$  (or the neutron and the proton).

$$\begin{aligned} R_v &= \frac{Y_p^{\pi^+} - Y_p^{\pi^-}}{Y_d^{\pi^+} - Y_d^{\pi^-}} \\ &= \sigma^p / \sigma^d \frac{R_p^{\pi^+} - R_p^{\pi^-}}{R_d^{\pi^+} - R_d^{\pi^-}}, \end{aligned} \quad (45)$$

$$\begin{aligned} R_s &= \frac{Y_p^{\pi^-} - Y_n^{\pi^-}}{Y_p^{\pi^+} - Y_n^{\pi^+}} \\ &= \frac{R_p^{\pi^-} - \sigma^n / \sigma^p R_n^{\pi^-}}{R_p^{\pi^+} - \sigma^n / \sigma^p R_n^{\pi^+}}, \end{aligned} \quad (46)$$

with  $R_{p(d,n)} = Y_{p(d,n)}^{\pi^{+(-)}} / Y_{p(d,n)}^{e^-}$  being the relevant multiplicities.

As the inclusive cross section ratio  $\sigma^d/\sigma^p$  (for the  $x$  range of this experiment,  $0.1 < x < 0.5$ , the neutron to proton cross section ratio  $\sigma^n/\sigma^p$  can be easily derived from  $\sigma^d/\sigma^p$ ) is one of the best known quantities in deep-inelastic scattering, and we will measure it without any additional effort in the electron arm of the experiment anyway, we will determine the relative normalization between our measured pion yields from a comparison of our own inclusive measurement of this cross section ratio and the known ratio  $\sigma^d/\sigma^p$ . Following this approach, we will not only avoid the (relatively) large uncertainties in the determination of the densities of the cryogenic targets (presently estimated to be 0.8%), but at the same time eliminate other uncertainties effecting this normalization. These include uncertainties due to beam charge measurements, any inefficiencies for electron detection and possible target boiling effects. The normalization of the measured inclusive cross section ratio to a well known quantity incorporates all these effects at the same time.

As already indicated above, the only quantity we need to monitor with high precision is the ratio of the inclusive electron yields on the two different targets. Given the high rates of such inclusive measurements (compared to the measurement of semi-inclusive pion yields at selected pion momenta), the statistics of this measurement certainly is only an issue of setting up a suitable trigger. Even though details on the trigger settings need to be worked out, it should be noted that similar prescaling procedures have been used for a long time at Hall C at lower energies and have been shown to be well under control.

Thus the normalization procedure and uncertainty ultimately becomes a question of

- How well can we measure the inclusive cross section ratio ?
- What's the present knowledge of the ratio  $\sigma^d/\sigma^p$  ?

On the first point, we plan to use the usual Hall C strategy to determine the inclusive cross sections of the deuteron and the proton, i.e. to correct the measured yields for beam charge, target densities, acceptance, dead time, efficiencies and radiative effects. The resulting cross section ratio will then be compared to the "world" knowledge of  $\sigma^d/\sigma^p$  and the relative normalization of the deuteron and proton yields determined.

The main systematic uncertainty in this procedure is the accuracy of the subtraction of radiative effects. However, as the kinematic range of this measurement is restricted to a region with relatively small radiative effects, the resulting uncertainty is expected to be very small. A first estimate indeed resulted into an uncertainty of less than 0.12 % for hydrogen and 0.09 % for deuterium, resulting into a maximal uncertainty in the ratio of 0.15 % .

The existing knowledge of the cross section ratio  $\sigma^d/\sigma^p$  is rather impressive. Because of various experiments at CERN, SLAC and DESY, a large body of data exists and has been found to be consistent with each other. The highest precision data have been provided by the NMC experiment [33] which quotes typical systematic uncertainties of 0.2 % and a normalisation uncertainty of  $\sigma^d/\sigma^p$  of 0.1 %. A very recent analysis of all available data [34] has resulted into a high precision description of the cross section ratio which covers the large kinematic range of  $0.002 < x < 0.85$ ,  $0.1 < Q^2 < 100 \text{ GeV}^2$  and  $0.25 < \epsilon < 1.0$ . The main body of data to be collected at this experiment lies in the region of the SLAC experiments which have small point-to-point systematic uncertainties. The main uncertainty in those data is related to their overall normalization uncertainty which effectively got removed by the renormalization of the SLAC data within the global analysis of all existing data (there is a large overlap between the SLAC data and the much more precise NMC data).

We thus believe we should be able to determine the relative normalization of the pion yields measured in this experiment to better than 0.25-0.3 %.

### 3.6 Events and background rates estimation

The estimation of the coincidence cross sections has the following inputs:

- The inclusive (e,e') cross sections for proton and deuteron.
- A parameterization of the favored and unfavored fragmentation functions  $D^+(z)$  and  $D^-(z)$  as a function of  $Q^2$ .
- a model of the transverse momentum distributions of pion as fragmentation products.

The inclusive deep inelastic (e,e') cross-section can be expressed in the quark parton model as:

$$\frac{d^2\sigma}{d\Omega dE'} = \frac{\alpha^2(1 + (1 - y)^2)}{sxy^2} \frac{E'}{m_N\nu} \sum_i e_i^2 (q_i(x, Q^2) + \bar{q}_i(x, Q^2)) \quad (47)$$

where  $m_N$  is the nucleon mass,  $y = \nu/E$ ,  $s = 2Em_N + m_N^2$ . The quark distribution  $q_i(x, Q^2)$  and  $\bar{q}_i(x, Q^2)$  are taken from the CTEQ6M [35] global fits and MRST2004 [36] global fits.

At leading twist and leading order, the semi-inclusive (e,e'h) cross-section relates to the quark fragmentation function  $D_q^h(z)$  and the total inclusive cross-section  $\sigma_{tot}$  through:

$$\frac{1}{\sigma_{tot}} \frac{d\sigma(e, e'h)}{dz} = \frac{\sum_i e_i^2 f_i(x, Q^2) D_i^h(z, Q^2)}{\sum_i e_i^2 f_i(x, Q^2)} \quad (48)$$

The two light quark fragmentation functions,  $D^+(z, Q^2)$  and  $D^-(z, Q^2)$ , relate to each other approximately by [37]:

$$D'(z) = \frac{D^-(z, Q^2)}{D^+(z, Q^2)} = \frac{1-z}{1+z}. \quad (49)$$

HERMES data [38] show some deviation from the above approximation, which can be parameterized [39] as  $D'(z) = (1-z)^{0.008358}/(1+z)^{1.984}$ . The fragmentation functions, such as  $D^\pi(z, Q^2) = (D^+(z, Q^2) + D^-(z, Q^2))/2$ , were from BKK parameterization [24] based the world  $e^+e^-$  data. The recent HERMES results [40] show that the pion transverse momentum ( $p_{hT}$ ) distribution follows the form of  $e^{-bp_{hT}^2}$  with  $b = 4.661 \pm 0.024 \text{ GeV}^{-2}$  for  $\pi^-$  production. We used the above HERMES results and realistic spectrometer acceptances to estimate the count rates. In this proposal, the hadron arm HMS is close to the  $\vec{q}$  direction (low transverse momentum).

The estimated coincident rates are listed in Table. 5 for the hydrogen and the deuterium target. We also estimated the singles rate for HMS and SHMS for each kinematic setting. For HMS, we used Whitlow [41], Rosetail [42, 43], Wiser [44], and pos-Wiser to estimate the singles electron rate, hadron rate and the positron rate, respectively. For SHMS, we used Whitlow [41], QFS of Lightbody and O'Connell [45] and Wiser [44] to estimate the electron and  $\pi^-$  rates. The SHMS single rates on hydrogen and deuterium target can be found in Table. 7 and Table. 8, respectively. The HMS single rates on detecting positive charged particle and detecting negative charged particle can be found in Table. 9 and Table. 10, respectively. The signal to background ratio in the worst case is better than 4.0 for  $\pi^\pm$  and 4.0 for  $k^\pm$  taking into account a 1.2 ns coincidence timing window.

### 3.7 Running time allocation and choice of luminosity

Time distribution is chosen to minimize statistical uncertainties of  $r_2$  ( $d_v/u_v$ ) which is the cleanest quantity within NLO QCD correction. The time distribution for the low hadron arm momentum setting, middle hadron arm momentum setting and high hadron arm momentum setting is 20%, 70% and 10%, respectively. This time distribution plan will be enough to check the LO  $x - z$  factorization assumption for different  $z$  bins. Meanwhile, most of time will be spent in the middle  $z$  range within which the LO  $x - z$  factorization has been proved by experiments. We assume 1008 hours (42 days) for production data. The detailed time distribution can be found in Table. 6. A total 52 days of beam time which includes six days for calibration, target changes and spectrometer momentum setting and polarity changes and four days of aluminum dummy running is requested.

The choice of luminosity for different kinematics setting can be seen at Table. 1. It is based on following considerations:

- The current on deuterium target is half of that on hydrogen target in order to keep a similar background rate in HMS and SHMS.
- The current for positive charged particle detection and the current for negative charged particle detection are chosen to have a similar total rates in hadron arm (HMS). This choice can minimize the systematic error due to the tracking efficiency of HMS which is the largest systematic uncertainty in calculating the

Target	$p_{SHMS}$ . GeV/c	$p_{HMS}$ GeV/c	(e,e' $\pi^+$ ) Hz	(e,e' $\pi^-$ ) Hz	(e,e' $K^+$ ) Hz	(e,e' $K^-$ ) Hz
LH	6.3	1.8	9.99	13.5	0.849	1.09
LH	6.3	2.2	24.5	29.9	2.84	3.20
LH	6.3	2.7	54.4	58.8	8.40	8.01
LH	6.4	1.8	5.46	7.32	0.444	0.558
LH	6.4	2.2	13.6	16.5	1.55	1.71
LH	6.4	2.7	31.2	33.3	4.88	4.57
LH	6.1	1.8	2.17	2.99	0.173	0.224
LH	6.1	2.25	6.30	7.67	0.732	0.824
LH	6.1	2.85	17.9	18.7	2.97	2.75
LD	6.3	1.8	8.18	12.7	0.726	1.03
LD	6.3	2.2	19.9	28.8	2.38	3.00
LD	6.3	2.7	44.0	58.0	6.89	7.43
LD	6.4	1.8	4.16	6.51	0.355	0.492
LD	6.4	2.2	10.3	15.0	1.21	1.48
LD	6.4	2.7	23.3	31.2	3.69	3.84
LD	6.1	1.8	1.60	2.56	0.134	0.193
LD	6.1	2.25	4.57	6.75	0.552	0.692
LD	6.1	2.85	12.8	17.0	2.17	2.23

Table 5: SIDIS rates for  $\pi^\pm$  and  $K^\pm$ .

Target	$p_{HMS}$ GeV/c	$p_{SHMS}$ GeV/c	$T^+$ hrs	$T^-$ hrs
LH	6.3	1.8	9	5
LH	6.3	2.2	32	16
LH	6.3	2.7	5	2
LD	6.3	1.8	11	6
LD	6.3	2.2	39	21
LD	6.3	2.7	6	3
LH	6.4	1.8	15	7
LH	6.4	2.2	51	24
LH	6.4	2.7	7	3
LD	6.4	1.8	21	11
LD	6.4	2.2	74	38
LD	6.4	2.7	11	5
LH	6.1	1.8	30	13
LH	6.1	2.25	104	46
LH	6.1	2.85	15	7
LD	6.1	1.8	50	25
LD	6.1	2.25	173	88
LD	6.1	2.85	25	13

Table 6: Time distribution for different kinematics settings. Here  $T^+$  ( $T^-$ ) means time spend on positive (negative) polarity magnet setting of HMS.

yield. In this case, when we form ratio of the yields, the systematic error of this effect can be minimized.

- With a 1.2 ns coincident window, we chose the luminosity in order to achieve a signal to noise ratio better than 4.
- The beam current is kept below  $50 \mu\text{A}$  in order to have the target density fluctuation effect under control.

### 3.8 Systematics uncertainties

There are several sources for systematic errors.

- **Target related uncertainties** The first one is the target related error which is due to the difference between the hydrogen and the deuterium target. The dominant target related errors are the proton and deuteron relative luminosity correction and the target density fluctuation. Single arm inclusive data will be used to monitor the overall luminosity as described previously. To first order, the target density fluctuation will be canceled exactly by forming the yield ratio. Here a overall 0.35% target related error that contains second order effect from target density fluctuations and the uncertainties from the inclusive measurements are used in projections.
- **Charge related uncertainties** The second major source is charge related error which is due to the difference between the positive-charged particle and negative-charged particle detection. The uncertainties due to final state interactions can be minimized by choosing parallel kinematics and higher  $W'$  values to avoid the resonance region. Our choice of the pion momentum which is larger than  $1.7 \text{ GeV}/c$  will minimize the effect of the final state interaction, and a 0.5% uncertainties is assumed in the projection. For PID, we intentionally choose to have similar single rates in hadron arm for positive charged particle and negative charged particle to minimize the systematic error due to tracking in hadron arm. Since we plan to measure yield ratios rather than the absolute cross-sections, sensitivity to instrumental effects are minimized. A 0.5% uncerntainty is assumed due to the PID corrections.
- **Parton Distribution Functions and Fragmentation Functions input uncertainties** To extract the  $\bar{d}/\bar{u}$  ratio, several other systematic uncertainties will be introduced. The first one is due to the ratio of the fragmentation functions  $D'(z)$  ( $D^-/D^+$ ) when we form  $r(x, z)$ . In this experiment, we will measure this quantity precisely and have a global fit with world data (high energy  $e^+e^-$  data, HERMES data, EMC data, etc). The NLO  $Q^2$  evolution has been developed for the fragmentation function [24]. In our projections, we used our measured  $D'(z)$ . The uncertainties on  $D'(z)$  will include the statistical error, the charge related systematic error, the parton distribution function error, the uncertainties due to  $Q^2$  and  $z$  evolution. From the comparison of HERMES data ( $Q^2 = 2.3 \text{ GeV}/c^2$ ) and EMC data ( $Q^2 = 25 \text{ GeV}/c^2$ ) [38], no strong  $Q^2$  dependence were seen in the  $D'(z)$ . For different  $x$  bins, the  $z$  coverage will be similar which can minimize the systematic uncertainties from  $z$  dependence of  $D'(z)$ . The second one arises from the parton distribution input. When we form  $\bar{d} - \bar{u}$  and  $\bar{d}/\bar{u}$ , certain PDF inputs are needed. Here

we used the difference between the CTEQ6 and MRST2004 as the systematic error for all of our PDF inputs ( $u - d$ ,  $\bar{u} + \bar{d}$  and  $\bar{u} + u$ ).

- **Higher Twist effects** In general, considering the virtual photon polarization, the cross-section can be written as

$$\sigma = \epsilon\sigma_L + \sigma_T + \sqrt{2\epsilon(\epsilon+1)}\sigma_{LT}\cos(\phi_\pi) + \epsilon\sigma_{TT}\cos(2\phi_\pi) \quad (50)$$

where  $\epsilon$  is the virtual photon polarization and  $\phi_\pi$  is the pion azimuthal angle. The  $\sigma_T$  is in leading twist and leading order can be written as product of parton distribution function and fragmentation function within LO  $x - z$  factorization. The  $\sigma_L$  and  $\sigma_{LT}$  are higher twist effect, while  $\sigma_{TT}$  is in leading twist. Experiment E00-108 preliminary results [8] show a negligible  $\sigma_{TT}$  term while the  $\sigma_{LT}$  term is about 15% of  $\sigma_T$ . In 11 GeV case, we expect the contribution of higher twist effect become smaller compared with 6 GeV E00-108 experiment. The complete coverage in  $\phi_\pi$  for  $0.2 < x < 0.4$  (Fig. 10) should allow us to determine both the shape of the possible  $\phi_\pi$  dependence and its magnitude for both  $\pi^+$  and  $\pi^-$ . Within the limited coverage at lower values of  $x$ , we then should be able to use the information from higher  $x$  points to constrain the functional form and get a realistic estimate even within the limited  $\phi_\pi$  range at these lower  $x$  values. The limited  $\phi_\pi$  coverage will possibly enhance the statistical uncertainties on the extracted transverse cross-section. The effect of  $\sigma_L$  can not be obtained from this experiment. Another experiment [46] is being proposed in JLab Hall C at 11 GeV which will be dedicated to measure the longitudinal to transverse cross-section ratio  $R$ . For now, we can estimate this ratio from inclusive DIS data. In this case, the  $R$  is the same for  $\pi^+$  and  $\pi^-$ . A reanalysis of SLAC DIS data on e-p and e-d scattering performed between 1970 and 1985 shows that  $R^p = R^d$  [47]. The effects of higher twist longitudinal cross-section are canceled completely when forming yield ratio between hydrogen and deuterium  $\pi^\pm$  productions.

- **Effects due to Limited Transverse Momentum Coverage**

A limited transverse momentum coverage (Fig. 11) can lead to a difference between  $\pi^\pm$  detection when the transverse momentum dependent favored and unfavored fragmentation functions are different ( $D'(z)$ ), where we assume that the transverse momentum dependence of parton distribution functions for different quark flavors are same. JLab Hall B [48] can perform a precise measurement of the transverse momentum dependence of favored and unfavored fragmentation functions at 11 GeV. We estimated that this systematic error is less than 0.5% from Cahn effect [49, 50] with Hall B's precise measurement. From Eqn.6 and Eqn.7 the transverse momentum dependence by assuming a full azimuthal coverage can be written as:

$$\sigma \approx [1 + (1 - y)^2] \frac{\exp(-\frac{P_{hT}^2}{\mu_D^2 + \mu_0^2 z^2})}{\mu_D^2 + \mu_0^2 z^2} \sum_q e_q^2 f_1^2(x) D_q^h(z) \quad (51)$$

We did the estimation of this systematic error based on the expected Hall B measurement [48] on  $\mu_D^{fav}$  and  $\mu_D^{unfav}$ .

In method II, the effect of limited transverse momentum coverage won't appear in the formula due to the complete cancellation of fragmentation function. In method I, this effect will emerge when we extract the fragmentation ratio.

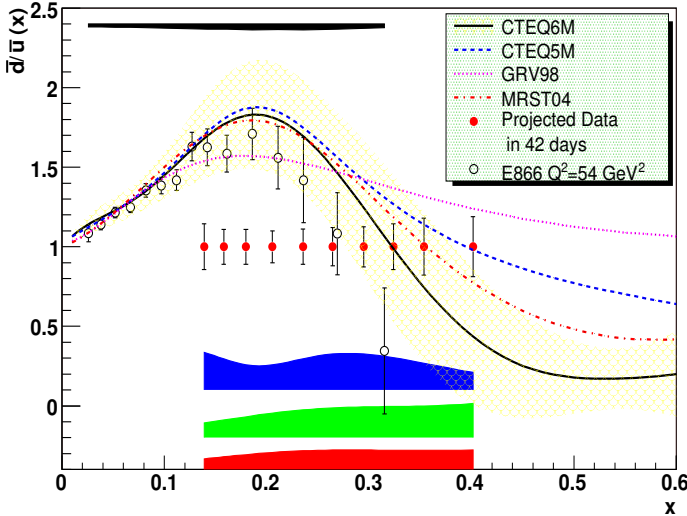


Figure 17: The projected uncertainties in the extraction of  $\bar{d}/\bar{u}$  in Hall C with a 11 GeV/c incident electron beam. The published E866 results are plotted for comparison. The red band shows the target related uncertainties. The green band shows the charge related uncertainties and fragmentation ratio related uncertainties. The blue band shows the uncertainties due to PDF input in forming  $\bar{d}/\bar{u}$ .

- **NLO Effects in Leading Order Analysis** Theorists [10] are currently carrying out a calculation of the QCD NLO corrections to SIDIS processes at the JLab 11 GeV kinematics. We anticipate that a completely new method will be performed at NLO QCD level by the time the data are available from the proposed experiment.

Systematic errors are shown as error band in all projections in the next section. In particular, all different systematic uncertainties are categorized in Fig. 17. At low  $x$ , the dominant errors are charge related and CTEQ input related errors; while at high  $x$ , the charge related and the target related errors contribute more. From Fig. 17, it is clear that the systematic errors are dominant in this experiment.

### 3.9 Projections

The projected results were obtained from a Monte Carlo [51] based on the CTEQ Low- $Q^2$  parton distribution parameterizations [52], the LUND string fragmentation model [53], and a model of the expected spectrometer acceptance in Hall C. We compared the rate from this Monte Carlo simulation and data, the difference is smaller than 30% in all kinematics. A overall detecting efficiency of 95% is assumed in the projection for both pion and Kaon.

The projections of  $r_1$  and  $r_2$  are shown in Fig. 18 and Fig. 19. We will also test the LO  $x - z$  factorization assumption; the statistical uncertainties of  $r_1$ ,  $r_2$ ,  $r_h$  and  $D'(z)$  are shown in Fig. 21 and Fig. 20.

For extended flavor asymmetry variables  $((\bar{d} - \bar{u})/(u - d)$ ,  $\bar{d} - \bar{u}$  and  $\bar{d}/\bar{u}$ ), only the results of Method II are presented here, the results of Method I can be found

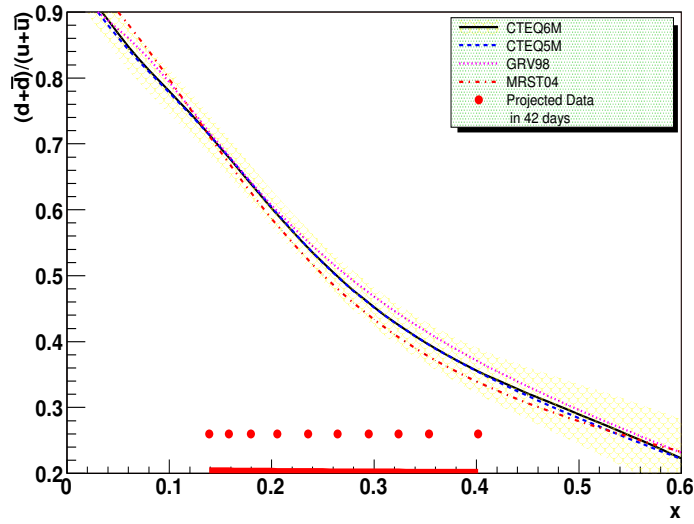


Figure 18: The projected uncertainties of  $r_1 = \frac{d+\bar{d}}{u+\bar{u}}$  in Hall C with a 11 GeV/c incident electron beam. We compared our projections with different parton distribution function parameterizations.

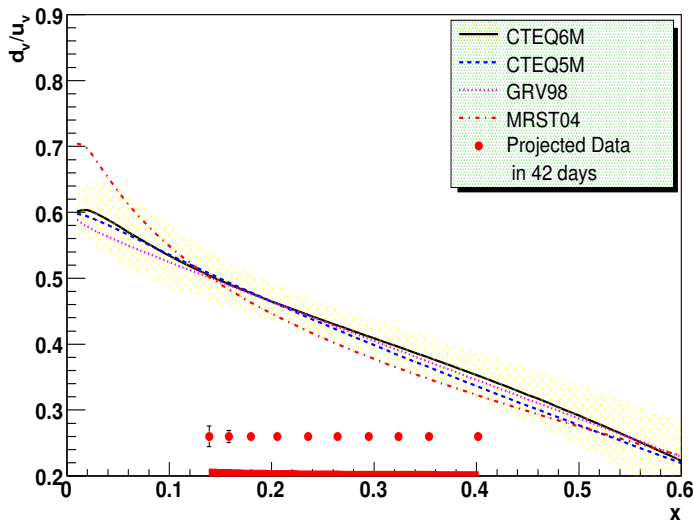


Figure 19: The projected uncertainties of  $r_2 = \frac{d_v}{u_v}$  in Hall C with a 11 GeV/c incident electron beam. We compared our projections with different parton distribution function parameterizations.

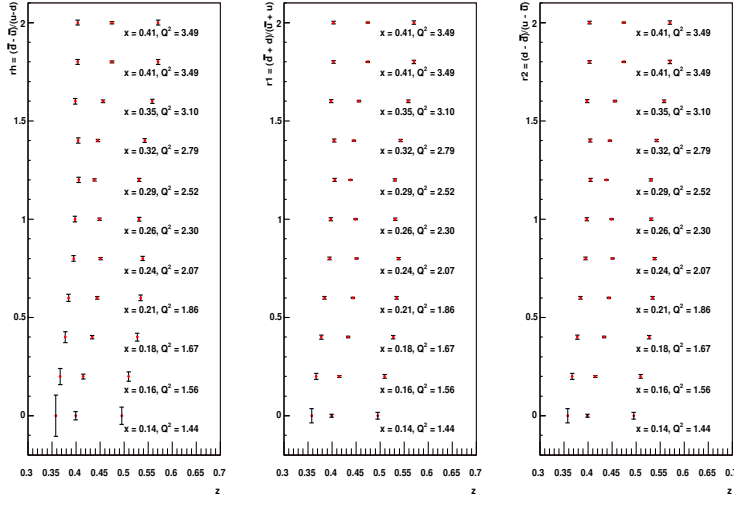


Figure 20: In order to test the factorization assumption, we will study the  $z$  dependence for  $r_1 = \frac{d+\bar{d}}{u+\bar{u}}$ ,  $r_2 = \frac{d_v}{u_v}$  and  $r_h = \frac{\bar{d}-\bar{u}}{u-\bar{d}}$  within different  $x$  bins. Only statistical error are presented here.

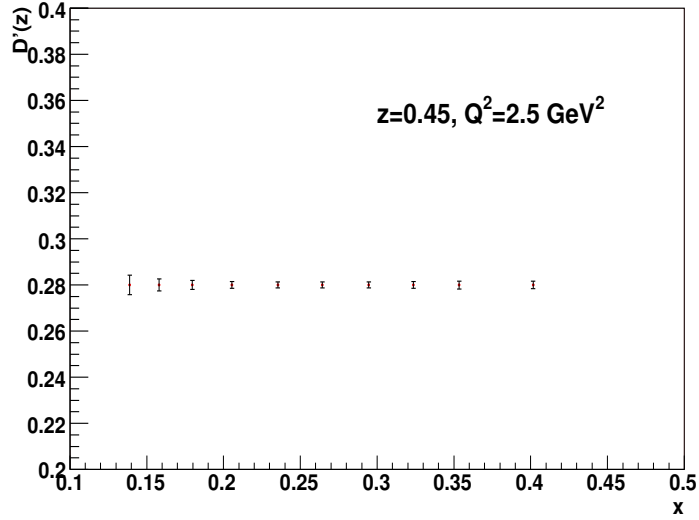


Figure 21: In order to test the factorization assumption, we will also study the  $x$  dependence for  $D'(z)$ . Only statistical error are shown here.

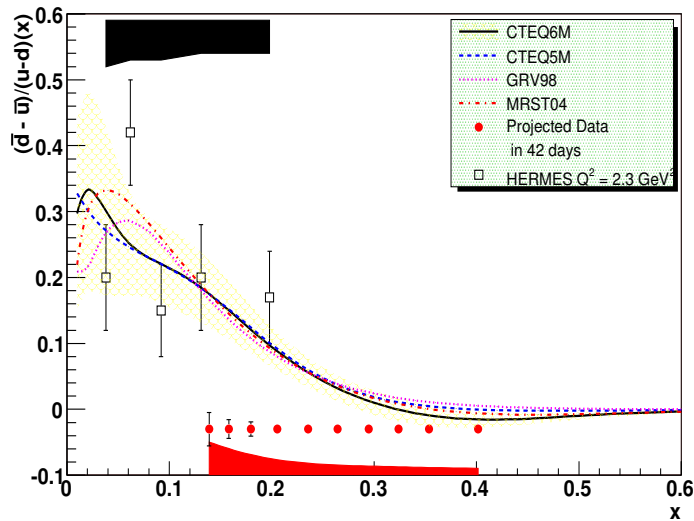


Figure 22: The projected uncertainties in the extraction of  $(\bar{d} - \bar{u})/(u - d)$  in Hall C with a 11 GeV/c incident electron beam. The published HERMES results are plotted for comparison. The systematic uncertainties are shown as the error band. Different parton distribution function parameterization are also presented for comparison.

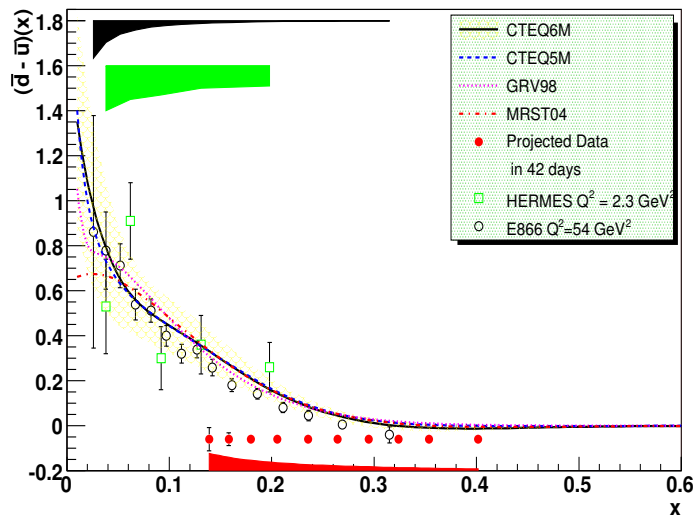


Figure 23: The projected uncertainties in the extraction of  $\bar{d} - \bar{u}$  in Hall C with a 11 GeV/c incident electron beam. The published results from E866 and HERMES are plotted for comparison. The systematic uncertainties are shown as the error band. Different parton distribution function parameterization are also presented for comparison.

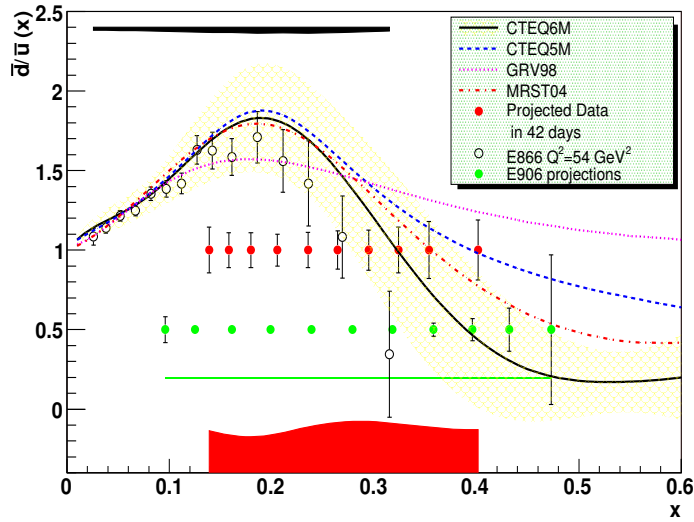


Figure 24: The projected uncertainties in the extraction of  $\bar{d}/\bar{u}$  in Hall C with a 11 GeV/c incident electron beam. The published E866 results are plotted for comparison. The projections for E906 experiment are also plotted for comparison. The systematic uncertainties are shown as the error band. Different parton distribution function parameterization are also presented for comparison.

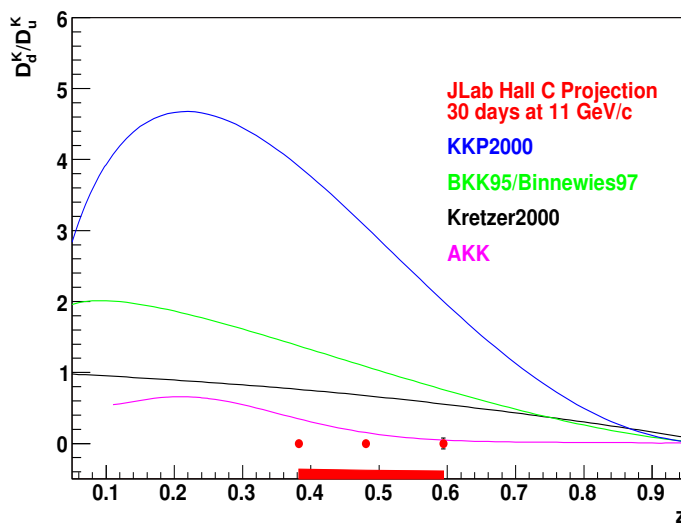


Figure 25: Projections in the determination of the Kaon fragmentation function ratio together with four parameterizations of the fragmentation functions fit to the  $e^+e^-$  data.

in Appendix B. The projected uncertainties in the extraction of the  $(\bar{d} - \bar{u})/(u - d)$  are presented in Fig. 22. By using  $u - d$  and  $\bar{u} + \bar{d}$ , projected uncertainties in the extraction of  $\bar{d} - \bar{u}$  and  $\bar{d}/\bar{u}$  are presented in Fig. 23 and Fig. 24, respectively. However, compared with the existing Drell-Yan data the systematic uncertainties from SIDIS measurements become very important in the high  $x$  region due to the dominance of the valence quark contribution. Fig. 25 shows the expected precision of the measurement of the ratio  $D_d^K/D_u^K$ . The four curves are parameterizations [27, 24, 54, 55, 56] of the fragmentation functions which fit to the  $e^+e^-$  data.

While Drell-Yan measurements have unique sensitivity probing the sea quark contribution to the nucleon structure, semi-inclusive deep-in-elastic measurements provide complementarity to Drell-Yan measurements.

## 4 Summary

A study of the light quark sea flavor asymmetry in the high  $x$  region with statistical precision comparable to the E866 Drell-Yan measurement and exceeding HERMES measurement is achievable with a 12 GeV CEBAF. Though the incident electron energy is lower than that available at HERMES, the larger scattering angle allows for an exploration of a similar  $Q^2$  range with much higher precision. The average Jefferson Lab  $Q^2$  value is much smaller than that of the E866 data, which will provide a possible sensitivity to  $Q^2$  dependence of the parton distribution functions. The proposed  $x$  range of our SIDIS measurement will overlap well with the  $x$  range of the planned new Drell-Yan experiment E906 [57] at Fermi Lab. This measurement would allow for a more detailed high statistical check of the LO  $x - z$  factorization assumption at 11 GeV. Results of sea quark ratio  $\bar{d}/\bar{u}$  will provide an independent study of the interesting drop in this ratio with increasing  $x$  at  $x > 0.15$ . The high precision measurement of  $(\bar{d} + d)/(\bar{u} + u)$  and  $d_v/u_v$  will provide strong constraints on parton distribution functions. In addition, these measurements will open a window to considerably more physics opportunities with SIDIS. The study of kaon production will provide information on kaon fragmentation function ratio which has never been studied before experimentally.

## 5 Acknowledgment

We thank B. Tipton's contribution in the early stage of this work, and Paul Reimer for providing the E906 experiment projections.

## 6 Appendix A: Single rates on HMS and SHMS

Target	detector	$p_{SHMS}$ GeV/c	$p_{HMS}$ GeV/c	polarity	$e^-$ kHz	$\pi^-$ kHz	$K^-$ kHz
LH	SHMS	6.3	1.8	+	8.50	2.60	0.238
LH	SHMS	6.3	1.8	-	18.5	5.65	0.517
LH	SHMS	6.3	2.2	+	15.2	4.66	0.426
LH	SHMS	6.3	2.2	-	32.5	9.97	0.911
LH	SHMS	6.3	2.7	+	27.6	8.46	0.773
LH	SHMS	6.3	2.7	-	57.8	17.7	1.62
LH	SHMS	6.4	1.8	+	4.88	0.839	0.0815
LH	SHMS	6.4	1.8	-	11.2	1.92	0.187
LH	SHMS	6.4	2.2	+	9.30	1.60	0.155
LH	SHMS	6.4	2.2	-	21.2	3.65	0.355
LH	SHMS	6.4	2.7	+	18.5	3.18	0.309
LH	SHMS	6.4	2.7	-	42.0	7.22	0.702
LH	SHMS	6.1	1.8	+	2.03	0.342	0.339
LH	SHMS	6.1	1.8	-	4.74	0.801	0.792
LH	SHMS	6.1	2.25	+	4.36	0.737	0.0729
LH	SHMS	6.1	2.25	-	10.1	1.71	0.169
LH	SHMS	6.1	2.85	+	10.6	1.79	0.177
LH	SHMS	6.1	2.85	-	24.2	4.10	0.405

Table 7: Singles rates for  $e^-$ ,  $\pi^-$  and  $K^-$  in SHMS for hydrogen target.

Target	detector	$p_{SHMS}$ GeV/c	$p_{HMS}$ GeV/c	polarity	$e^-$ kHz	$\pi^-$ kHz	$K^-$ kHz
LD	SHMS	6.3	1.8	+	7.43	2.58	0.235
LD	SHMS	6.3	1.8	-	16.1	5.59	0.511
LD	SHMS	6.3	2.2	+	13.3	4.61	0.421
LD	SHMS	6.3	2.2	-	28.4	9.86	0.900
LD	SHMS	6.3	2.7	+	24.1	8.34	0.764
LD	SHMS	6.3	2.7	-	50.5	17.5	1.6
LD	SHMS	6.4	1.8	+	4.05	0.830	0.0806
LD	SHMS	6.4	1.8	-	9.28	19.01	0.185
LD	SHMS	6.4	2.2	+	7.73	15.8	0.154
LD	SHMS	6.4	2.2	-	17.6	3.61	0.351
LD	SHMS	6.4	2.7	+	15.4	3.15	0.306
LD	SHMS	6.4	2.7	-	34.9	7.14	0.694
LD	SHMS	6.1	1.8	+	1.63	0.339	0.0335
LD	SHMS	6.1	1.8	-	3.81	0.793	0.0784
LD	SHMS	6.1	2.25	+	3.41	0.729	0.0721
LD	SHMS	6.1	2.25	-	8.13	1.69	0.167
LD	SHMS	6.1	2.85	+	8.40	1.77	0.174
LD	SHMS	6.1	2.85	-	19.5	4.05	0.401

Table 8: Singles rates for  $e^-$ ,  $\pi^-$  and  $K^-$  in SHMS for deuterium target.

Target	detector	$p_{HMS}$ GeV/c	$p_{SHMS}$ GeV/c	$\pi^+$ kHz	$K^+$ kHz	$p$ kHz	$e^+$ Hz	Total kHz
LH	HMS	1.8	6.3	204.7	23.65	60.99	57.39	289.4
LH	HMS	2.2	6.3	252.2	36.47	78.95	56.44	367.6
LH	HMS	2.7	6.3	269.7	48.80	89.24	47.64	407.9
LH	HMS	1.8	6.4	170.6	22.49	67.11	46.71	260.2
LH	HMS	2.2	6.4	195.9	32.31	83.55	42.56	311.8
LH	HMS	2.7	6.4	194.4	39.86	89.86	33.07	324.2
LH	HMS	1.8	6.1	161.2	21.93	68.14	43.83	251.3
LH	HMS	2.25	6.1	187.4	32.64	87.29	39.32	307.3
LH	HMS	2.85	6.1	184.3	41.09	94.68	29.00	320.1
LD	HMS	1.8	6.3	202.5	23.39	60.34	55.74	286.3
LD	HMS	2.2	6.3	249.5	36.08	78.11	54.81	363.7
LD	HMS	2.7	6.3	266.9	48.28	88.28	46.27	403.5
LD	HMS	1.8	6.4	168.7	22.25	66.39	45.35	257.4
LD	HMS	2.2	6.4	193.8	31.97	82.65	41.33	308.5
LD	HMS	2.7	6.4	192.4	39.45	88.89	32.12	320.7
LD	HMS	1.8	6.1	159.4	21.69	67.41	42.56	248.6
LD	HMS	2.25	6.1	185.4	32.29	86.36	38.18	304.1
LD	HMS	2.85	6.1	182.3	40.65	93.72	28.16	316.7

Table 9: Singles rates for  $e^+$ ,  $\pi^+$ ,  $K^+$  and proton in HMS for positive polarity.

Target	detector	$p_{HMS}$ GeV/c	$p_{SHMS}$ GeV/c	$\pi^-$ kHz	$K^-$ kHz	$e^-$ kHz	Total kHz
LH	HMS	1.8	6.3	274.2	13.22	4.761	292.2
LH	HMS	2.2	6.3	344.1	19.43	8.250	371.9
LH	HMS	2.7	6.3	372.7	24.62	14.77	412.1
LH	HMS	1.8	6.4	244.4	12.92	3.217	260.6
LH	HMS	2.2	6.4	290.1	18.02	5.861	314.0
LH	HMS	2.7	6.4	297.2	21.54	11.30	329.9
LH	HMS	1.8	6.1	236.3	12.72	2.959	252.0
LH	HMS	2.25	6.1	284.4	18.31	5.986	308.7
LH	HMS	2.85	6.1	288.6	22.10	13.80	324.5
LD	HMS	1.8	6.3	271.3	13.08	4.609	289.0
LD	HMS	2.2	6.3	340.6	19.23	8.210	368.0
LD	HMS	2.7	6.3	368.7	24.36	14.96	408.1
LD	HMS	1.8	6.4	241.8	12.78	3.105	257.7
LD	HMS	2.2	6.4	287.0	17.83	5.796	310.6
LD	HMS	2.7	6.4	293.9	21.32	11.36	326.6
LD	HMS	1.8	6.1	233.9	12.58	2.856	249.3
LD	HMS	2.25	6.1	281.4	18.11	5.929	305.4
LD	HMS	2.85	6.1	285.5	21.86	13.89	321.3

Table 10: Singles rates for  $e^+$ ,  $\pi^+$ ,  $K^+$  and proton in HMS for negative polarity.

## 7 Appendix B: Projections of Method I

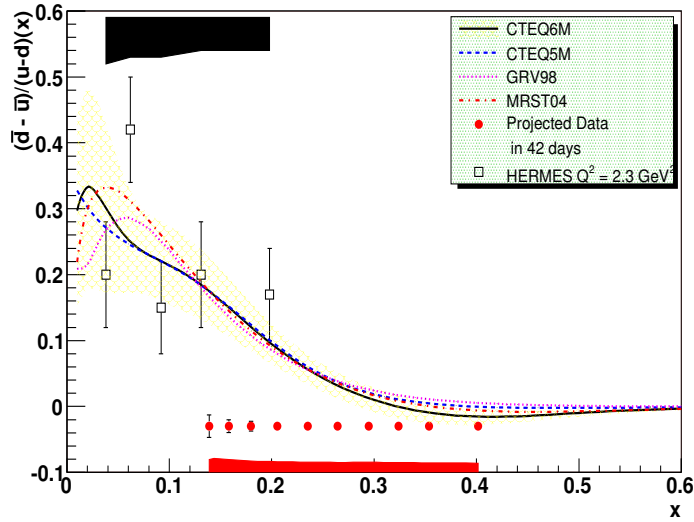


Figure 26: The projected uncertainties in the extraction of  $(\bar{d} - \bar{u})/(u - d)$  in Hall C with a 11 GeV/c incident electron beam. The published HERMES results are plotted for comparison. The systematic uncertainties are shown as the error band. Different parton distribution function parameterization are also presented for comparison.

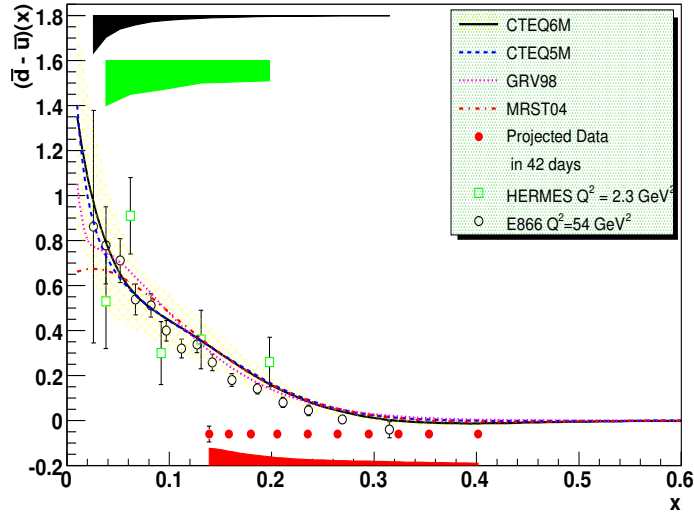


Figure 27: The projected uncertainties in the extraction of  $\bar{d} - \bar{u}$  in Hall C with a 11 GeV/c incident electron beam. The published results from E866 and HERMES are plotted for comparison. The systematic uncertainties are shown as the error band. Different parton distribution function parameterization are also presented for comparison.

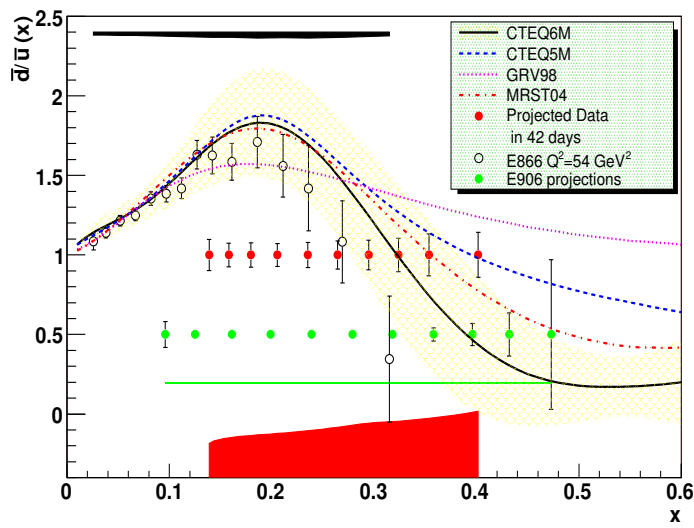


Figure 28: The projected uncertainties in the extraction of  $\bar{d} - \bar{u}$  in Hall C with a 11 GeV/c incident electron beam. The published E866 results are plotted for comparison. The projections of E906 experiment are also plotted for comparison. The systematic uncertainties are shown as the error band. Different parton distribution function parameterization are also presented for comparison.

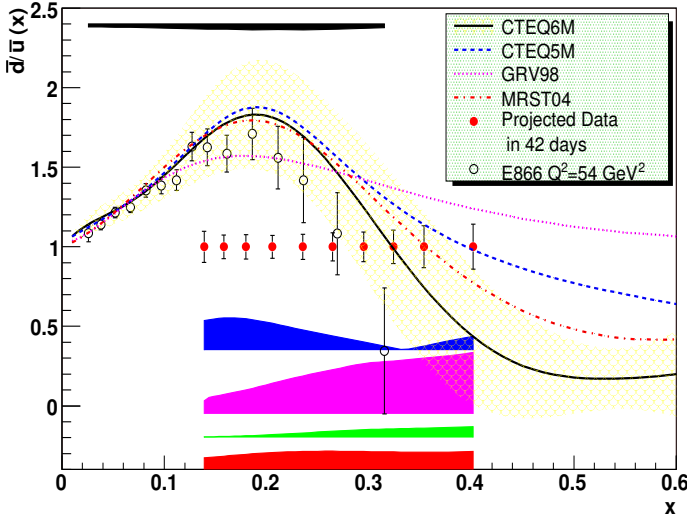


Figure 29: The projected uncertainties in the extraction of  $\bar{d}/\bar{u}$  in Hall C with a 11 GeV/c incident electron beam. The published E866 results are plotted for comparison. The red band shows the target related uncertainties. The green band shows the charge related and fragmentation ratio related uncertainties. The blue band shows the uncertainties due to PDF inputs in forming  $\bar{d}/\bar{u}$ .

## References

- [1] J. C. Collins, *Nucl. Phys.* **B396**, 161 (1993).
- [2] J. Levelt *et al.*, *Phys. Lett.* **B263** 498 (1991).
- [3] HERMES Collaboration, K. Ackerstaff *et al.*, *Phys. Rev. Lett.* **81** 5519 (1998).
- [4] E866 Collaboration, E. A. Hawker *et. al.*, *Phys. Rev. Lett.* **80** 3715 (1998); R. S. Towell *et al.*, *Phys. Rev.* **D64** 052002 (2001).
- [5] W. Melnitchouk, J. Speth and A. W. Thomas, *Phys. Rev.* **D59** 014033 (1999).
- [6] R. K. Ellis, H. Georgi, M. Machacek, H. D. Politzer and G. G. Ross, *Nucl. Phys.* **B152** 285 (1979).
- [7] P. J. Mulders and R. D. Tangerman, *Nucl. Phys.* **B461** 197 (1996).
- [8] R. Ent, H. Mkrtchyan and G. Niculescu, JLab E00-108 “Duality in Meson Electroproduction”.
- [9] H. Avakian *et al.* *Phys. Rev.* **D69** 112004 (2004), hep-ex/0301005.
- [10] W. Vogelsan, F. Yuan, private communication.
- [11] For a review see e.g. R. Vogt, *Prog. Part. Nucl. Phys.* **45** S105 (2000).
- [12] K. Gottfried, *Phys. Rev. Lett.* **18** 1174 (1967).
- [13] P. Amaudruz, *et al.*, *Phys. Rev. Lett.* **66** 2712 (1991).
- [14] S. Kumano, *Phys. Rep.* **303** 183 (1998).
- [15] J. Speth and A. W. Thomas, *Adv. Nucl. Phys.* **24** (1998).

- [16] G. T. Garvey and J. C. Peng, *Prog. Part. Nucl. Phys.* **47**, 203 (2001).
- [17] J. C. Collins *et al.*, hep-ph/0409313, *Adv. Ser. Direct High Energy Phys.* 5 1-91 (1988).
- [18] X. D. Ji, J. P. Ma and F. Yuan, *Phys. Rev.* **D71** 034005 (2005), hep-ph/0404183.
- [19] E. L. Berger, J. W. Qiu and X. F. Zhang, *Phys. Rev.* **D65** 034006 (2002), hep-ph/0107309.
- [20] D. Graudenz, *Nucl. Phys.* **B432** 351 (1994).
- [21] A. Bacchetta, *Phys. Lett.* **B574** 225 (2003), hep-ph/0307282.
- [22] D. de Florian, C. A. Garcia Canal and R. Sassot, *Nucl. Phys.* **B470** 195 (1996).
- [23] M. Glück, *et al.* *Z. Phys. C* **67** 433 (1995).
- [24] J. Binnewies, B. A. Kniehl and G. Kramer, *Phys. Rev.* **D52** 4947 (1995).
- [25] D. de Florian, O. A. Sampayo and R. Sassot *Phys. Rev.* **D57** 5803 (1998).
- [26] D. de Florian, G. A. Navarro and R. Sassot *Phys. Rev.* **D71** 094018 (2005).
- [27] B. A. Kniehl, G. Kramer and B. Potter, *Nucl. Phys.* **B582** 514 (2000), hep-ph/0010289.
- [28] R. Ent and H. Mkrtchyan, private communications.
- [29] M. Alberg, E. M. Henley and G. A. Miller, *Phys. Lett.* **B471** 396 (2000).
- [30] W. Melnitchouk, J. Speth and A.W. Thomas, *Phys. Rev.* **D59** 014033 (1998).
- [31] P.J. Mulders, AIP Conf. Proc. 588 (2001) 75-88, hep-ph/0010199, “Current fragmentation in semi-inclusive leptonproduction”.
- [32] T. Sloan, G. Smadja and R. Voss, *Phys Rep.* **162** 46 (1988).
- [33] NMC collaboration, M. Arneodo et al, *Phys. Lett.* **91**, 062001 (2003).
- [34] Presentation at HERMES collaboration meeting, Oct 2005.
- [35] J. Pumplin *et al.* JHEP 07 012 (2002), hep-ph/0201195.
- [36] A. D. Martin *et al.*, *Phys. Lett.* **B636**, 259 (2006), hep-ph/0603143.
- [37] R. D. Field and R. P. Feynman, *Nucl. Phys.* **B136** 1 (1978).
- [38] P. Geiger, Ph.D Thesis (2003).
- [39] D. Gaskell, private communication.
- [40] B. Hommez, Ph.D Thesis (2003).
- [41] L. W. Whitlow, SLAC-Report-357 (1990).
- [42] Mo and Tsai, *Rev. Mod. Phys.* **41** 205 (1969).
- [43] Stein *et al.* *Phys. Rev.* **D12** 1884 (1975).
- [44] D. E. Wiser, Ph.D. thesis, Univ. of Wisconsin (1977).
- [45] J. W. Lightbody, Jr., J. S. O' Connell, Computers in Physics May/June (1988).
- [46] Rolf Ent and Hamlet Mkrtchyan, private communication.
- [47] L. W. Whitlow *et al.* *Phys. Lett.* **B250** 193 (1990).

- [48] H. Avakian, private communication.
- [49] R. N. Cahn, *Phys. lett.* **B78** 269 (1978).
- [50] M. Anselmino *et al.* *Phy. Rev.* **D71** 074006 (2005), hep-ph/0501196.
- [51] G. Ingleman, A. Edin and J. Rathsmann, DESY Report 96-057 (1996).
- [52] H. L. Lai *et. al.*, *Phys. Rev.* **D55** 1280 (1997).
- [53] T. Sjöstrand, *Comp. Phys. Comm.* **83** 74 (1994).
- [54] S. Kretzer, *Phys. Rev.* **D62** 054001 (2000), hep-ph/0003177.
- [55] J. Binnewies, DESY report 97-128, hep-ph/9707269.
- [56] S. Albino, B. A. Kniehl and G. Kramer *Nucl. Phys.* **B725** 181 (2005), hep-ph/0502188.
- [57] Drell-Yan measurements of nucleon and nuclear structure with the FNAL main injector, spokesperson: D.F. Geesaman and P. Reimer.